Lung epithelial signaling mediates early vaccine-induced CD4$^+$ T cell activation and *Mtb* control

Shibali Das[1#], Nancy D. Marin[1#], Ekaterina Esaulova[2], Mushtaq Ahmed[1], Amanda Swain[2], Bruce A. Rosa[3], Makedonka Mitreva[3,4], Javier Rangel-Moreno[5], Mihai G Netea[6,7], Luis B. Barreiro[8], Maziar Divangahi[9], Maxim N. Artyomov[2], Deepak Kaushal[10], and Shabaana A. Khader[1]*

[1]Department of Molecular Microbiology, Washington University in St. Louis, St. Louis, MO, USA

[2]Department of Pathology and Immunology, Washington University in St. Louis, St Louis, MO, USA

[3]Department of Medicine, Division of Infectious Diseases, Washington University in St. Louis, St. Louis, MO, USA

[4]McDonnell Genome Institute, Washington University in St. Louis, St. Louis, MO, USA

[5]Department of Medicine, Division of Allergy, Immunology and Rheumatology, University of Rochester Medical Center, Rochester, NY, USA

[6]Department of Internal Medicine, Radboudumc Center for Infectious Diseases, Nijmegen, Netherlands.

[7]Department of Immunology and Metabolism, Life and Medical Sciences Institute, University of Bonn, Bonn, Germany.

[8]Department of Medicine, Genetic Section and, University of Chicago, Chicago, IL, USA

[9]Meakins-Christie Laboratories, Department of Medicine, Department of Microbiology and Immunology, Department of Pathology, McGill University Health Centre and McGill International TB Centre, McGill University, Montreal, QC, Canada.

[10]Southwest National Primate Research Center, Texas Biomedical Research Institute, San Antonio, TX, USA

[#]Co-first authors.

*****For Correspondence:

Shabaana A. Khader

Department of Molecular Microbiology,

Washington University in St. Louis,

St. Louis, MO, USA

Email: sakhader@wustl.edu

Key words: Tuberculosis, vaccine-induced response, clonality, parenchyma, epithelial cells, cytokines.

Running Title: Epithelial signaling mediates vaccine *Mtb* control

Abstract

Tuberculosis (TB) is one of the leading causes of death due to a single infectious agent. The development of a TB vaccine that induces durable and effective immunity to *Mycobacterium tuberculosis* (*Mtb*) infection is urgently needed. Early and superior *Mtb* control can be induced in *M. bovis* Bacillus Calmette–Guérin (BCG) vaccinated hosts when the innate immune response is targeted to generate effective vaccine-induced immunity. In the present study, we show that innate activation of DCs is critical for mucosal localization of clonally activated vaccine-induced $CD4^+$ T cells in the lung, and superior early *Mtb* control. In addition, our study reveals that Th1/Th17 cytokine axis play an important role in superior vaccine induced immunity. Our studies also show that activation of nuclear factor kappa-light-chain-enhancer of activated B cells (NFκβ) pathway in lung epithelial cells is critical for the mucosal localization of activated vaccine-induced $CD4^+$ T cells for rapid *Mtb* control. Thus, our study provides novel insights into the immune mechanisms that can overcome TB vaccine bottlenecks and provide early rapid *Mtb* control.

Importance: Tuberculosis is a leading cause of death due to single infectious agent accounting 1.4 million deaths each year. The only licensed vaccine BCG is not effective due to variable efficacy. In our study, we determined the early immune events necessary for achieving complete protection in BCG vaccinated host. Our study reveals that innate activation of DCs can mediate superior and early *Mtb* control in BCG vaccinated host through lung epithelial cell signaling and localization of clonal activated, *Mtb* antigen specific, cytokine producing $CD4^+$ T cells within the lung parenchyma and airways. Thus, our study provides novel insights into the immune mechanisms that can overcome TB vaccine bottlenecks and provide early rapid *Mtb* control.

Introduction

Mycobacterium tuberculosis (*Mtb*) is a leading cause of death worldwide by a single infectious agent and it infects approximately one fourth of the world's population (1). Currently, *M. bovis* Bacillus Calmette-Guerin (BCG) is the only licensed vaccine against tuberculosis (TB). However, the variable efficacy of BCG, along with the emergence of drug resistant *Mtb* strains and comorbidity associated with Human Immunodeficiency Virus infection, has further confounded the eradication of TB as a public health problem. Recently, the M72/AS01E vaccine has been reported to provide about 50% efficacy in *Mtb*-infected adults against pulmonary TB disease (2). Additionally, use of BCG vaccination either mucosally or intravenously (IV) in rhesus macaques substantially limited *Mtb* infection (3-5). However, despite these break-through findings in the TB vaccine field, we do not fully understand the mechanistic basis behind the early immune events within the lungs that mediates protection in vaccinated hosts.

T cells are required to control *Mtb* in vivo as mice lacking $CD4^+$ T cells are unable to control *Mtb* infection (6). *Mtb* infection is known to delay initiation of the adaptive T cell immune response resulting in early uncontrolled *Mtb* growth (7-9). Moreover, during *Mtb* infection, the colocalization of immune cells, including $CD4^+$ T cells and macrophages within the lung parenchyma rather than in the lung vasculature is critical for early *Mtb* control (10, 11). However, the exact mechanisms that mediate the recruitment of $CD4^+$ T cells in vaccinated hosts to mediate *Mtb* control is unclear. In the current study, using a mouse model of early superior *Mtb* control in BCG vaccinated hosts, we have delineated the early protective mechanisms that mediate vaccine-induced *Mtb* control. We demonstrate that the localization of clonally expanded *Mtb*-specific cytokine-producing $CD4^+$ T cell population which preferentially localize in the lung parenchyma and airways, are critical for early *Mtb* control. Additionally, early signaling events in lung epithelial cells are critical to facilitate the interaction between activated *Mtb*-specific $CD4^+$ T cells and macrophages, within the parenchyma and airways, for rapid *Mtb*

control in this model. Thus, our study provides novel immunological insights into the early mechanism of vaccine-induced protective immunity against TB, allowing for potential targeting these pathways to improve TB vaccine efficacy for future use.

Results

Innate activation of DCs amplifies clonal vaccine-induced CD4$^+$ T cell responses in *Mtb*-infected BCG vaccinated host

Delayed activation and accumulation of *Mtb*-specific vaccine-induced T cells in the lung is a critical bottleneck for vaccine protection against *Mtb* infection (8, 9). Innate activation by transfer of exogenously zymosan activated *Mtb* antigen 85B (Ag85B)-pulsed DCs (Z-DC) into BCG vaccinated *Mtb*-infected hosts resulted in early CD4$^+$ T cell recruitment, enhanced IFN-γ and IL-17 production and complete early control of *Mtb* replication in mice (8). Using this published model of early and superior vaccine-induced *Mtb* control, we probed the exact immune mechanism(s) of protection in vaccinated hosts. The peak of the CD4$^+$T cell response in unvaccinated *Mtb*-infected mice is 20 dpi, while the peak of the vaccine response is 15 dpi following *Mtb* infection (12). We also showed that in Vac+Z-DC group, the vaccine responses are accelerated at 8 and 15 dpi (8). Therefore, we picked the peak time point as the appropriate measurement of effective T cell responses between the conditions in order to assess their full expression of antimycobacterial function. As a first step, lung cells were isolated at the peak of the immune response respectively from *Mtb*-infected unvaccinated C57BL/6 mice at 20 days post infection [dpi] (Unvac), *Mtb*-infected BCG vaccinated C57BL/6 mice at 15 dpi (Vac), and *Mtb*-infected BCG vaccinated C57BL/6 mice that received Z-DC transfer (given intratracheally at -1 and +4 dpi) at 8 and 15 dpi (Vac+Z-DC) (**Fig.1A**) and subjected to single cell RNA sequencing (scRNA-Seq) to define the immune cell populations driving enhanced vaccine-induced immunity.

In CD3$^+$ cells, unsupervised clustering yielded four clusters of CD4$^+$ cells, namely naive CD4$^+$ (*Ccr7*$^+$*Sell*$^+$), two clusters of effector CD4$^+$ cells (*Ccr7*$^-$*Sell*$^-$*CD44*$^+$ or *Ifng*$^+$) and T regulatory cells

(Foxp3$^+$); three clusters of CD8$^+$ cells - naive CD8$^+$ (*Ccr7*$^+$*Sell*$^+$), cytotoxic CD8$^+$ (*Gzmb*$^+$*Prf1*$^+$), mix of CD8$^+$ and Tγδ cells; and more enriched Tγδ cluster (*Trgv2*$^+$) (**Fig. 1B, C and Fig. S1A, Table S1**). Notably, cluster of naive CD4$^+$ T cells dominated in both *Mtb*-infected unvaccinated and BCG vaccinated mice and decreased in *Mtb*-infected BCG vaccinated mice that received Z-DC transfer (40% versus 20% of T cells). In contrast, effector CD4_1 cluster dominated the T cell population in *Mtb*-infected BCG vaccinated mice that received Z-DC transfer (harvested at either 8 or 15 dpi) while being almost absent in *Mtb*-infected BCG vaccinated or unvaccinated mice (35-55% versus <10% of total T cells, **Fig. 1D and S1B**). Effector CD4_1 exhibited the signature of lung T resident memory (Trm) cells including *Cxcr3, Cxcr6, Itgae, Cd44, Cd69 and Cd101*(13) (**Fig. 1E and Fig. S1C**). We have used the publically available surface receptor markers of Trm cells in lungs of humans as broad lung T cell tissue resident signature (13, 14). Gene set enrichment analysis (GSEA) shows an enrichment of genes, upregulated in lung Trm (GSE94964), in our comparison between CD4_1 and CD4_2/Naive CD4 clusters. Incidentally, we also identified TCR for each cell, and first compared clonotype expansion with Gini coefficient (coefficient of 0 means that each T cell clonotype has only 1 T cell, while coefficient of 1 means that all T cells have identical clonotype). CD4$^+$ cells from *Mtb*-infected BCG vaccinated mice that received Z-DC transfer had Gini coefficient twice higher than *Mtb*-infected unvaccinated or BCG vaccinated mice, suggesting that *Mtb*-infected BCG vaccinated mice that received Z-DC transfer have more expanded clonotypes, when compared to CD4$^+$ T cells in *Mtb*-infected unvaccinated or BCG vaccinated mice (**Fig. 1F**).

We also identified potential motif-based groups of CD4$^+$ T cells recognizing the same epitopes derived from antigens among the TCRs using TCRdist tool. We focused on the 3 most well-defined motifs with conserved amino acids, coming from TCR clusters of size 108, 19 and 49 TCRs (**Fig. 1G,H, Fig S1D and Table S2**). As TCRdist operates on unique TCR sequences without taking into account clonotype expansion, we enumerated the number of CD4$^+$ T cells

expressing any of these TCR motifs, and we found that motif 1 was exclusively associated with *Mtb*-infected BCG vaccinated mice that received Z-DC transfer, where it was present in 10-25% of all $CD4^+$ T cells (**Fig. 1I**, left panel **and Fig. S1E**), while other motifs were much less expanded. Motif 1 is characterized by TRAV3-3 - TRAJ27/37/52 - TRBV16 pairing, and it features sub-motifs in both CDR3α and CDR3β. Conserved amino acids come from V and J gene parts rather than from insertion of random nucleotides. Furthermore, we found that majority of cells with motif 1 belonged to effector CD4_1 cluster (**Fig. 1I,** right panel), accounting for >20% of cells inside the cluster. We next analyzed transcriptional differences among the $CD4^+$ T cells between different groups. Therefore, we isolated the $CD4^+$ T cells (at the time of peak $CD4^+$ T cell responses) from *Mtb*-infected unvaccinated C57BL/6 mice at 20 dpi, *Mtb*-infected vaccinated C57BL/6 mice at 15 dpi and *Mtb*-infected vaccinated C57BL/6 mice that received Z-DC transfer at 8 dpi (**Fig. 1J and Fig. S2A**). Among the top 25 differently expressed genes in the *Mtb*-infected BCG vaccinated mice that received Z-DC transfer, there was a marked upregulation of genes associated with T cell migration including *Ccr8 (15), Itgae (Cd103)* (16)*, Aqp3* (17) and *Rbpj* associated with cell-cell communications (18). Surprisingly, gene expression profile of $CD4^+$ T cells from *Mtb*-infected unvaccinated or BCG vaccinated mice were comparable (**Fig. 1J**, **Fig. S2A and B**). The important enriched pathways associated with T cells receptor signaling and T cell function were observed in the *Mtb*-infected BCG vaccinated mice that received Z-DC transfer compared with the $CD4^+$ T cells isolated from BCG vaccinated mice (**Fig. S2C**). Therefore, our data suggest that $CD4^+$ T cells that confer early *Mtb* control in *Mtb*-infected BCG vaccinated mice that received Z-DC transfer express functionally distinct T cell transcriptional profiles associated with migration.

Early activation and mucosal localization of $CD4^+$ T cells mediates improved *Mtb* control in BCG vaccinated host

We next determined the functional ability of the vaccine-induced $CD4^+$ T cells to promote macrophage killing of *Mtb*. We isolated highly pure lung $CD4^+$ T cells from either *Mtb*-infected

BCG vaccinated C57BL/6 mice (at 15 dpi) or *Mtb*-infected BCG vaccinated C57BL/6 mice that received Z-DC transfer (at 8 dpi) and co-cultured isolated $CD4^+$ T cells with *Mtb*-infected macrophages in vitro to assess *Mtb* killing. Interestingly, both $CD4^+$ T cells from *Mtb*-infected BCG vaccinated mice and *Mtb*-infected BCG vaccinated mice that received Z-DC transfer effectively mediated comparable *Mtb* killing (**Fig. 2A**). Additionally, while IFN-γ production was similar in supernatants from co-cultures of both groups that received $CD4^+$ T cells (**Fig. 2B**), higher levels of IL-17 were detected in co-cultures that received $CD4^+$ T cells from *Mtb*-infected BCG vaccinated mice that received Z-DC transfer, when compared to co-cultures that received *Mtb*-infected BCG vaccinated $CD4^+$ T cells (**Fig. 2C**). As we did not find any functional differences in *Mtb* killing within macrophages between the two groups, we hypothesized that the clonally expanded $CD4^+$ T effector population was mediating improved protection possibly due to other mechanisms rather than just direct activation of macrophages. Thus, we next isolated highly pure lung $CD4^+$T cells from *Mtb*-infected vaccinated mice that received Z-DC transfer (at 8 dpi) and adoptively transferred the $CD4^+$ T cells into the BCG vaccinated C57BL/6 mice following *Mtb* infection, while control mice were BCG vaccinated and *Mtb*-infected that did not receive T cells. The rationale was to test if adoptive transfer improved *Mtb* control when compared with just BCG vaccination. Adoptive transfer of purified $CD4^+$ T cells into *Mtb*-infected BCG vaccinated mice resulted in improved *Mtb* control, when compared to PBS treated *Mtb*-infected BCG vaccinated mice (**Fig. 2D**), and this coincided with improved B cell follicle formation associated with immune control of *Mtb* (19), without impacting overall lung inflammation (**Fig. 2E and F**). This improved *Mtb* control coincided with dampened production of proinflammatory cytokines in the lungs of Mtb-infected BCG vaccinated mice that received $CD4^+$ T cells including IL-12, TNF-α, IL-10, IL-1β and IL-6, and the chemokines KC, MIP-1β, RANTES and MIP-2 (**Fig. 2G and H**) corroborating with the unaltered overall lung inflammatory landscape. Together, these results suggest that vaccine-induced $CD4^+$ T cell drive protection in

188 *Mtb*-infected BCG vaccinated hosts likely by their ability to migrate and localize into specific lung
189 compartments. Therefore, we next studied the kinetics associated with the $CD4^+$ T cell
190 activation as well as localization of $CD4^+$ T cells in the lung of *Mtb*-infected BCG vaccinated
191 mice and *Mtb*-infected BCG vaccinated mice that received Z-DC transfer. Remarkable $CD4^+$ T
192 cell activation ($CD44^{hi}$) was observed as early as 3 dpi (**gating strategy in Fig. S2D)** in *Mtb*-
193 infected BCG vaccinated mice that received Z-DC transfer, and this correlated with significant
194 and rapid accumulation of *Mtb* Ag85B tetramer-specific (TET^+) $CD4^+$ T cells (within the lungs of
195 *Mtb*-infected BCG vaccinated mice that received Z-DC transfer compared to *Mtb*-infected BCG
196 vaccinated mice **(Fig. 3A, and Fig. S3A**). These robust and early responses were maintained,
197 with 8 dpi being the peak of the response. We observed nearly 400-fold higher
198 $CD4^+CD44^{hi}TET^+$ T cells in *Mtb*-infected BCG vaccinated mice that received Z-DC transfer,
199 when compared with *Mtb*-infected BCG vaccinated mice. In contrast, the expansion and
200 accumulation of $CD4^+CD44^{hi}TET^+$ T cells in *Mtb*-infected BCG vaccinated mice was delayed
201 until 20 dpi (**Fig. 3A).**
202 Immune cell recruitment in airways and parenchyma correlated with increased protection
203 compared to localization in lung vasculature during *Mtb* infection (11, 20). To identify the
204 localization of activated T cells to specific lung compartments, we tracked vasculature-
205 localization (CD45.2-$BV605^+$), airway localization (CD45.2-$V500^+$) and parenchyma localization
206 (BV605 negative V500 negative) of immune cells in the lung (10, 11, 21) by administering anti-
207 CD45.2-BV605 intravascularly or anti-CD45.2-V500 intratracheally just prior to sacrifice. We
208 found that $CD4^+CD44^{hi}$ (**Fig. S3B**), $CD4^+CD44^{hi}TET^+$ T cells (**Fig. 3B**) localized to the lung
209 parenchyma of *Mtb*-infected BCG vaccinated mice that received Z-DC transfer at very early time
210 points (3-15 dpi), with progressive accumulation of $CD4^+CD44^{hi}$ and $CD4^+CD44^{hi}TET^+$ T cells
211 into the airways over time. Coincident with the delayed accumulation of $CD4^+CD44^{hi}TET^+$ T cells
212 in *Mtb*-infected BCG vaccinated mice, the majority of the $CD4^+CD44^{hi}TET^+$ T cells localized
213 mainly in vasculature and parenchyma with some cells localizing within the airways (**Fig. 3B,**

inset). These data together suggest that activation of the innate immune pathways to target vaccine-induced T cell responses can initiate rapid expansion of $CD4^+CD44^{hi}TET^+$ T cells with specific localization in the lung parenchyma and airways, contributing to early and rapid *Mtb* control.

CXCR3 is a well-described chemokine receptor expressed by circulating T cells. As infection progressed, the accumulation of $CD4^+CD44^{hi}TET^+CXCR3^+$ T cells increased into the lung parenchyma and airways in *Mtb*-infected BCG vaccinated mice that received Z-DC transfer (**Fig. 3C)**. However, reduced accumulation of $CD4^+CD44^{hi}TET^+CXCR3^+$ T cells in the lung parenchyma and airways in *Mtb*-infected BCG vaccinated mice was observed (**Fig. 3C, inset)**. The $CD4^+CD44^{hi}TET^+CXCR3^+$ cells which expanded at d15 post infection exhibited a ratio of parenchyma: vasculature associated T cells of 16.69 (± 10.54) in Vac+Z-DC mice as compared with BCG vaccinated mice (3.794 ± 6.572, p 0.0489 by Student's T test between Vac+Z-DC and BCG vaccinated *Mtb*-infected mice). IFN-γ and IL-17 are important effector cytokines that contribute to protective immune responses against *Mtb* infection (3, 22, 23). While the majority of the $CD4^+CD44^{hi}TET^+$ T cells were $IL\text{-}17^+$ cytokine-producing, a population of $IFN\text{-}\gamma^+$ cytokine-producing and $IFN\text{-}\gamma^+$ /$IL\text{-}17^+$ double cytokine-producing $CD4^+CD44^{hi}TET^+$ T cells were also found in the lungs of *Mtb*-infected vaccinated mice that received Z-DC transfer and they accumulated as early as 5 dpi with peak responses at 8 dpi (**Fig. 3D**). Importantly, the cytokine-producing $CD4^+CD44^{hi}TET^+$ T cells predominantly localized to the lung parenchyma and airways. Moreover, in *Mtb*-infected BCG vaccinated mice that received Z-DC transfer, the frequency of $IL\text{-}17^+$ cytokine-producing $CD4^+CD44^{hi}TET^+$ T cells showed an early and sustained increase, when compared with $IFN\text{-}\gamma^+$ and $IFN\text{-}\gamma^+IL\text{-}17^+$ cytokine-producing $CD4^+CD44^{hi}TET^+$ T cells. Indeed, consistent with delayed accumulation of $CD4^+CD44^{hi}TET^+$ T cells in *Mtb*-infected BCG vaccinated lungs, the number of $IFN\gamma^+$ and $IL\text{-}17^+$ single or dual cytokine-producing $CD4^+CD44^{hi}TET^+$ T cells were delayed and 10 fold lower in *Mtb*-infected BCG vaccinated mice,

and they preferentially localized in the vasculature (**Fig. 3E**). To fully characterize the role of cytokine signaling in Z-DC mediated protection in the BCG vaccinated *Mtb* infected mice, we transferred Z-DC in BCG vaccinated IL-17/IL-22 double knockout (*Il-17/Il-22*$^{-/-}$) mice with or without IFN-γ neutralization to evaluate the specific contribution of Th1 and/or Th17 responses. Absence of IL-17/IL-22 signaling together led to significantly higher bacterial burden (**Fig. 3F**) as compared with the wild type BCG vaccinated C57BL/6 mice, which also received Z-DC transfer. These results suggest an important role for IL-17/IL-22 signaling, specifically under conditions of the superior protection enabled by Z-DC transfer in BCG vaccinated mice. Additionally, we observed reduced expression of MHC-II expression on alveolar macrophages (AMs) (**Fig. 3G, gating strategy in Fig. S3C**) within the lung of BCG vaccinated *Il-17/Il-22*$^{-/-}$ mice receiving Z-DC transfer. Moreover, blocking IFN-γ in BCG vaccinated *Il-17/Il-22*$^{-/-}$ mice which also received Z-DC transfer, abrogates *Mtb* control with significant reduction in expression of MHC Class II expression on AMs and reduced accumulation of $CD4^{+}CD44^{hi}TET^{+}$ T cells, compared with the wild type BCG vaccinated C57BL/6 mice receiving Z-DC transfer (**Fig. 3G,H**). Therefore, our study points towards a synergistic role played by the Th1-Th17 axis in mediating better protection in the BCG vaccinated *Mtb* infected mice receiving Z-DC. These results suggest that the protection mediated in the *Mtb*-infected BCG vaccinated mice that received Z-DC transfer is associated with an early activation, expansion and localization of cytokine-producing $CD4^{+}$ T cells within the parenchyma and airways where *Mtb*-infected macrophages are harbored.

Both scRNA-Seq and bulk gene signature analysis of $CD4^{+}$ T cells demonstrated elevated expression of genes associated with migration such as *Itgae* or the genes expressed by tissue resident T cells such as the chemokine receptor, *Ccr8* (**Fig. 1B and I**). Expression of CD103 and CCR8 on $CD4^{+}CD44^{hi}TET^{+}$ T cells peaked on 8 and 15 dpi respectively which corresponded with the enhanced recruitment of $CD4^{+}CD44^{hi}TET^{+}$ T cells into lungs and the early control of *Mtb* replication in BCG vaccinated mice that received Z-DC transfer (**Fig. 3I, J**

and insets). In addition, *Mtb*-infected *Cd103* deficient BCG vaccinated mice that received Z-DC transfer exhibited similar protective capacity than *Mtb*-infected wild type mice that also received Z-DC transfer (**Fig. S3D**), suggesting that CD103 expression did not induce additional protective mechanisms in BCG vaccinated mice that received Z-DC transfer. In contrast, *Ccr8* deficient *Mtb*-infected BCG vaccinated mice receiving Z-DC transfer did not control *Mtb* replication to the similar level as observed in wild type *Mtb*-infected BCG vaccinated mice that received Z-DC transfer (**Fig. 3K**). This decreased vaccine-induced control in *Ccr8* deficient *Mtb*-infected BCG vaccinated mice receiving Z-DC transfer coincided with reduced accumulation of $CD4^{+}CD44^{hi}TET^{+}$ T cells within the lung of *Ccr8* deficient mice (**Fig. 3L**). These results suggest CD103-independent but CCR8-dependent mechanisms underlying Z-DC mediated vaccine-induced *Mtb* control. However, it could also be possible that CCR8 along with CD103 synergistically regulate the $CD4^{+}$ T cell localization and activation to impact *Mtb* replication in vivo and needs further experimentation.

Lung epithelial signaling is critical for early immune cell activation and mucosal localization in *Mtb*-infected vaccinated mice

Our data demonstrate that mucosal localization of $CD4^{+}$ T cells within the parenchyma and airways is effective at inducing complete early *Mtb* control in vaccinated hosts. Our recent studies showed that AMs upon activation migrate from the airways into the parenchyma to form granulomas and mediate effective *Mtb* control (10). Thus, we next addressed if localization of $CD4^{+}$ T cells in the parenchyma and airways resulted in more effective and early activation of AMs. We observed that AMs readily accumulated in the lung airways and parenchyma of *Mtb*-infected BCG vaccinated mice that received Z-DC transfer (**Fig. 4A, gating strategy in Fig.S3C)** with increasing accumulation and rapid early upregulation of MHC Class II expression as an indicator of activation **(Fig. 4B)**. In contrast, AM localization within the airways in the *Mtb*-infected BCG vaccinated mice lungs was delayed with fewer AMs that accumulated within the parenchyma and delayed timing of AM activation. In BCG vaccinated mice, while there is no

significant accumulation of AMs in the parenchyma, there is a small but significant increase in AM population within the airways at 15 dpi, when compared to 8 dpi. Additionally, we observed a marked early recruitment and activation of recruited macrophages (RMs), mainly in airways and lung parenchyma of the *Mtb*-infected BCG vaccinated mice that received Z-DC transfer. In contrast, in the *Mtb*-infected BCG vaccinated mice, RMs localized mainly in vasculature and at lesser extent in parenchyma (**Fig. 4C and D**). Thus, collectively our data suggest that early infiltration and localization of myeloid cells within specific lung parenchyma are crucial factors for inducing superior vaccine-induced immunity.

Epithelial cells respond to IL-17/IL-22 (24-26) and secrete various antimicrobial peptides and several chemokines (27), that orchestrate recruitment of immune cells such as neutrophils, recruited monocytes and natural Th17 cells (28, 29) . Thus, we hypothesized that activation of epithelial signaling will participate in production of mediators involved in strategic immune cell localization and early control of *Mtb* infection. To further delineate mechanistic insight of the signaling pathways associated with the superior vaccine-induced immunity in *Mtb*-infected BCG vaccinated mice that received Z-DC transfer, we used $Ikk^{fl/fl}Sftp^{cre}$ mice which lack NFκB signaling specifically in lung type II epithelial cells and therefore do not upregulate the expression of necessary inflammatory cytokines or chemokines (10, 30). Absence of functional lung epithelial signaling in *Mtb-infected* BCG vaccinated $Ikk^{fl/fl}Sftp^{cre}$ mice that received Z-DC transfer did not provide the superior and early vaccine-induced *Mtb* control as compared with the *Mtb*-infected BCG vaccinated $Ikk^{fl/fl}$ littermate control mice that received Z-DC transfer (**Fig. 4E**). These data suggest that functional epithelial signaling plays an important role in inducing the superior protection specifically under conditions of Z-DC transfer into BCG vaccinated mice following *Mtb*-infection. Moreover, we observed reduced B cell follicle formation within the lungs of *Mtb*-infected BCG vaccinated $Ikk^{fl/fl}Sftp^{cre}$ mice that received Z-DC transfer compared to *Mtb*-infected BCG vaccinated littermate control mice that received Z-DC transfer (**Fig. 4F)**. To further investigate the influence of functional epithelial signaling on immune mechanisms, we studied

the immune cell localization in *Mtb*-infected BCG vaccinated *Ikk*$^{fl/fl}$*Sftp*^{cre} and littermate control mice that received Z-DC transfer. As expected, we observed reduced AM accumulation within lung parenchyma in *Mtb*-infected BCG vaccinated *Ikk*$^{fl/fl}$*Sftp*^{cre} mice that received Z-DC transfer as compared with *Mtb*-infected BCG vaccinated littermate controls mice that received Z-DC transfer (**Fig. 4G)**. Although we did not see any defects in the accumulation of RMs in *Mtb*-infected BCG vaccinated *Ikk*$^{fl/fl}$*Sftp*^{cre} mice that received Z-DC transfer (**Fig. 4H)**, we observed defective activation of RMs in *Mtb*-infected BCG vaccinated *Ikk*$^{fl/fl}$*Sftp*^{cre} mice that received Z-DC transfer as compared with *Mtb*-infected BCG vaccinated littermate control mice that received Z-DC transfer (**Fig. S3E)**. Moreover, we found a significant reduction in the number of CD4^{+}CD44^{hi} and CD4^{+}CD44^{hi}TET^{+} T cells present in lung parenchyma of *Mtb*-infected BCG vaccinated *Ikk*$^{fl/fl}$*Sftp*^{cre} mice that received Z-DC transfer as compared with *Mtb*-infected BCG vaccinated littermate control mice that received Z-DC transfer (**Fig. S3F,G and Fig. 4I**). Similarly, the number of CD4^{+}CD44^{hi}TET^{+}IL-17^{+} cytokine-producing T cells present in lung parenchyma of *Mtb*-infected BCG vaccinated *Ikk*$^{fl/fl}$*Sftp*^{cre} mice that received Z-DC transfer was significantly reduced compared with *Mtb*-infected BCG vaccinated littermate control mice that received Z-DC transfer (**Fig. 4J**). The number of CD4^{+}CD44^{hi}TET^{+}IFN-γ^{+} cytokine-producing CD4^{+} T cells present in lung airways and parenchyma of *Mtb*-infected BCG vaccinated *Ikk*$^{fl/fl}$*Sftp*^{cre} mice that received Z-DC transfer was lower, as compared with *Mtb*-infected BCG vaccinated littermate control mice that received Z-DC transfer although it was not statistically significant (**Fig. 4K**). Thus, our data suggest that activation of lung epithelial signaling regulates the environmental signals that mediate localization and amplification of Th17/Th1 responses within the site of infection to mediate early superior control of *Mtb* infection in the vaccinated host.

Discussion

The development of a TB vaccine that induces durable and effective immunity to *Mtb* infection is urgently needed. Previously, we have demonstrated that complete and early *Mtb* control can be

induced in BCG vaccinated hosts when the innate immune response is targeted to generate effective vaccine-induced immunity. In the present study, we show that the mechanisms by which activation of innate immunity results in superior *Mtb* control is through rapid and robust amplification of cytokine-producing vaccine-induced T cell responses and localization within the airways and parenchyma of BCG vaccinated hosts. Our studies also show that activation of NFκβ pathway in lung epithelial cells is an important early event that drives the localization of vaccine-induced $CD4^+$ vaccine-induced T cells within parenchyma and activation of myeloid cells, thus promoting the formation of protective iBALT structures within the lung and control of *Mtb* replication. Therefore, our study provides novel insights into the immune mechanisms that can overcome TB vaccine bottlenecks and provide early rapid *Mtb* control.

Mtb is a successful pathogen due to its ability to evade host immune responses. Studies have shown that following *Mtb* infection, delay in the activation of antigen specific $CD4^+$ T cell responses occurs likely due to *Mtb*'s ability to directly inhibit MHC-II trans activator expression, MHC–II expression and antigen presentation (31). BCG vaccination can generate systemic vaccine-induced T cell responses, but upon *Mtb* challenge, the accumulation of T cells to the lung although accelerated when compared with naïve hosts (day 15 when compared to day 20 in naïve), is still not sufficiently early or durable enough to provide complete protection against *Mtb* infection (8, 32). Therefore, as shown in our previous work(8) and by others (33), targeting the innate pathway through DC activation is one way to rapidly activate T cell responses to mediate early and rapid control. Our new studies shown here, demonstrate that the mechanisms by which innate DC activation overcomes the roadblock is by rapid amplification of early $CD4^+$ T cell responses by 5 days post *Mtb* challenge, and localization within airway and parenchyma compartments in the lung. That these $CD4^+$ T cells are recruited and localized within 5 days, is by far the earliest recruitment of vaccine-induced T cells responses to most vaccine strategies against TB. This early amplification is similar to what is seen in even after 30 days following BCG IV vaccination in NHPs where the heightened and lung-localized Trm cells

are considered to be a mechanism through which complete control of *Mtb* infection is mediated (3). In the current study, we show that adoptive transfer of peptide pulsed Z-DC into BCG vaccinated mice provides superior *Mtb* control. We have previously shown that following BCG vaccination (34), the accumulation of antigen-specific lung-resident cytokine-producing T cells in the lung is not as robust as amplification of antigen-specific T cells in the spleen and lymph nodes of vaccinated mice. Based on these data, we expect that adoptive transfer of Z-DC results in activation of antigen-specific T cells in the lymph nodes and possibly recruitment to the lung. However, we don't rule out the possibility of local proliferation of T cells following Z-DC transfer. Thus, our results along with recent studies including IV (3) and mucosal BCG use (5), suggest that overcoming the *Mtb* suppression-mediated of early immune responses is thus possible and generating lung-resident activated T cell pool should be a good strategy for improving vaccine-induced immunity against TB.

During *Mtb* infection, Ag85B is predominantly secreted during the early phase of infection and expression reduced by 3 weeks post infection, while ESAT-6 is expressed and secreted by *Mtb* during chronic phases of infection (35). Since we are interested in the early events post infection, we designed our study to activate innate immune responses to amplify BCG-vaccine induced Ag85B specific $CD4^+$ T cell responses against *Mtb* infection. Indeed, our results show that early amplification of Ag85B specific T cell responses resulted in complete control of *Mtb* infection. As several vaccine formulations including whole vaccines such as BCG and subunit vaccine such as H56/IC31 (36) and H56/CAF01 (37) include Ag85B as an antigen, our results suggest that targeting innate DC activation to rapidly amplify Ag85B-specific $CD4^+$ T cell responses may further improve upon protection elicited by these vaccines in animal models and should be robustly tested. Furthermore, our studies for the first time demonstrate that in fact the transcriptional profiles that are induced in BCG vaccine-induced $CD4^+$ T cell responses are comparable to $CD4^+$ T cells induced in unvaccinated *Mtb*-infected mice, suggesting that the quality of responses induced by BCG vaccination is not very different from *Mtb* infection. This is

in sharp contrast to the early amplification of vaccine-induced $CD4^+$ T cells found in BCG vaccinated hosts that undergo innate DC activation where there was a marked upregulation of genes associated with T cell migration and cell-cell communications, especially expression of genes such as Cd103 and Ccr8 which likely allow localization of effector T cells into lung compartment for optimal *Mtb* control. Thus, our results also provide novel insights that both the timing of arrival of $CD4^+$ T cells and the quality (cytokine production and upregulation of receptors and proteins enabling lung localization) of $CD4^+$ T cells are important for optimal *Mtb* control, compared to $CD4^+$ T cells induced by BCG vaccination that are not fully protective.

For the first time as far as we are aware, our study was able to identify potential motif-based groups of $CD4^+$ T cells recognizing the epitopes of same antigens among the TCRs. Our results showed that a motif was exclusively associated with T cells in *Mtb*-infected BCG vaccinated mice that received Z-DC transfer, where it was present in 10-25% of all $CD4^+$ T cells. These results suggest that innate DC activation of T cells along with amplification of $CD4^+$ T cell also allows for clonal expansion of activated Trm cells. Previous studies have demonstrated that in mice vaccinated with Ag85B had a skewed CDR3β length distribution with preferential use of TRBV16 and two CDR3βs namely CASSLEGDEQYF and CASSLEGDTQYF (32). Our studies have not only validated the presence of the CDR3β motifs but also identified the motif on CDR3α that are amplified in $CD4^+$ T cells from BCG vaccinated mice that also received Ag85B primed Z-DCs. Our studies identified 3 CDR3α and 3 CDR3β motifs highly represented in effector $CD4^+$ T cells from BCG vaccinated mice that also received Ag85B primed Z-DCs. From the available literature(38) the predominant Motif 1 appears to be specific for *Mtb* Ag85B. The presence of “LEG” motif in the TCR sequence specifically in TCRβ, identifies the TCR specific for Ag85B. Carpenter et al, 2017 showed the TCRβ repertoire of vaccine-elicited ($Ag85B_{240-254}$) and *Mtb*-recalled Ag85b-specific $CD4^+$ T cells, as well as after primary infection.

Therefore, unlike the unvaccinated or BCG vaccine induced TCR repertoire on $CD4^+$ T cells, Z-DC induced TCR repertoire demonstrated in this study represents novel motifs which have potential to control *Mtb* infection. Thus, while bulk RNA-seq studies do not allow us due to the pooled nature of cells to understand the heterogeneity of T cell responses, scRNA-Seq allows us to understand the heterogeneity of T cell responses. For example, our results show that while activated population of clonally expanded $CD4^+$ T cells expressing Trm markers increase in BCG vaccinated host receiving Z-DC transfer, this population is not different between BCG vaccinated and unvaccinated lungs. Instead, an IFN-γ^+ $CD4^+$ T cell population is increased in BCG vaccinated lungs when compared with unvaccinated lungs. Therefore, our results highlight the utility of using single cell TCR sequencing to probe the expansion and clonality of vaccine-responsive $CD4^+$ T cells and provide an in-depth understanding of T cell responses generated following vaccination.

During *Mtb* infection, effective control of intracellular *Mtb* requires direct recognition of infected macrophages in the lung by $CD4^+$ effector T cells (39). Therefore, localization of Trm $CD4^+$ T cells in the lung is an important event required for *Mtb* control. CXCR3 expression on $CD4^+$ T cells ($CXCR3^+$) is considered a marker of lung recruited $CD4^+$ T cells and is important for localization of $CXCR3^+$ Th1 cells to the lung parenchyma (11). In contrast, a subset of $CD4^+$ Th1 cells that are highly differentiated ($Tbet^+$) and co-expressing $KLRG^+$ are present in the lung vasculature and are not efficient in controlling *Mtb* growth (11). Adoptive transfer of the less differentiated $CXCR3^+KLRG^-CD4^+$ purified parenchymal T cells provided protection upon *Mtb* challenge while the $CXCR3^+KLRG1^+$ T cells are not protective upon transfer. In human studies, $CXCR5^+$ $CCR5^+$ T cells in the lungs and pleural fluid produced IFN-γ (40-42). In preclinical macaque model of latent and active TB, $CXCR3^+CCR6^+$ co-expressing T cells produced both IL-17 and IFN-γ cytokines in the BAL and were associated with the protective responses in latent TB (43). Finally, in vaccine models of subunit vaccination, $CXCR3^+KLRG^-$ T cells readily

443 trafficked to the lung parenchyma and provided *Mtb* control (37). With the increased resolution
444 provided by our studies using a combination of IT and IV labeling, allow us to further
445 discriminate whether immune cells are localized within the airways or parenchyma or the
446 vascular compartments. Our studies using this new technique show that BCG vaccination
447 induces a mixed population of $CXCR3^+$ T cells that are distributed equally between the
448 vasculature, parenchyma and the airway compartments. In sharp contrast, BCG vaccinated
449 hosts that also receive Z-DC transfer show a remarkable enhancement of $CXCR3^+$ T cells that
450 localize within the airway and parenchyma compartments.
451 Our study show that upon BCG vaccination, the primary lung localizing T cells are IL-17
452 expressing cells that accumulate by day 15, with IFN-γ producing cells accumulating by day 21
453 post *Mtb* infection. In contrast, BCG vaccinated mice that receive Z-DC transfer recruit Th17
454 cells by 5 days mostly in the airways and parenchyma followed by IFN-γ-single or IFN-γ/IL-17-
455 coproducing cells accumulating largely in the airways and parenchyma by day 8. Both IFN-γ and
456 IL-17 have varied roles in *Mtb* control during vaccination. In the case of IFN-γ, while recent data
457 has shown that IFN-γ (44) and IFN-γ produced by $CD4^+$ T cells (21) are considered redundant,
458 IL-17 is necessary for vaccine-induced control in many models of vaccination (12, 34, 45). More
459 recent work from our lab has also demonstrated a critical role for IL-22 in mediating *Mtb* control.
460 Intriguingly in our model described here, our results show a combined role for IL-17/IL-22 and
461 IFN-γ in conferring early vaccine-induced control of *Mtb* infection. Therefore, it is likely that the
462 mucosal delivery of activated DCs accelerated parenchymal homing of antigen specific $CD4^+$ T
463 cell subsets to gain access to the *Mtb*-infected cells in the granuloma and reduce *Mtb* replication
464 through activation of signaling involving both Th1/Th17 cytokine axis.
465 Upregulation of *Itgae* (Cd103) and Ccr8 genes in $CD4^+$ T cells isolated from BCG vaccinated
466 *Mtb*-infected mice that received Z-DC transfer suggest that these molecules may regulate
467 $CD4^+$T cell migration and localization within the lung compartments. CD103 is an integrin highly

expressed in tissue resident memory T cells (21) and associated with epithelial retention of T cells through binding to E-cadherin expressed by epithelial cells (46). CD103 expressing T cells are present in lung and BAL but absent in blood of *Mtb* infected humans suggesting the fact that CD103 expressing cells are present at the site of *Mtb* infection. CD103 expressing T cells are enriched at the lung parenchyma and airways following mucosal vaccination with BCG or *Bacillus subtilis* spore fusion protein 1 (Spore-FP1) and confers better protection against *Mtb* infection compared to BCG parenteral vaccination (47, 48). Thus, retention of CD103 expressing T cells at the lung interface is likely necessary for providing protection against infection. Deficiency of Cd103 (in mice) correlated with reduced number of mucosal intraepithelial T cells (49). Our results show that despite the increased expression of CD103 on $CD4^+$ T cells isolated from BCG vaccinated *Mtb*-infected mice that received Z-DC transfer and localization within the airway and parenchyma, CD103 deficient mice upon BCG vaccination and Z-DC transfer still provided similarly superior protection as BCG vaccinated wild type C57BL/6 mice that received Z-DC transfer. These results suggest redundant features of integrin that may mask the effect of single deficiency of this protein, and compensatory mechanisms are being induced to ensure control of *Mtb* replication in CD103 deficient vaccinated mice that receive Z-DC transfer. Our studies also show for the first time that CCR8 expression is high on $CD4^+$ T cells isolated from BCG vaccinated mice receiving Z-DC transfer and expression is highest on airway localized Ag85b-specific $CD4^+$ T cells. CCR8 is commonly expressed by T regulatory subsets or T helper type 2 cells for efficient migration of T cell population to the site of inflammation (50). CCL1 was shown to be upregulated upon in vitro infection with *Mtb* and in patients with active tuberculosis versus latently infected controls (51, 52). However, the functional role of CCR8 expressing $CD4^+$ T cells during *Mtb* infection remains elusive. Our studies show a functional role for CCR8 expression in the superior protection mediated by the Z-DC transfer in BCG vaccinated mice, as absence of CCR8 expression abrogates Z-DC-mediated protection and accumulation of Ag85B-specific T cells. Together these results suggest

494 that CD103 and CCR8 have pivotal role to play in early $CD4^+$ T cell recruitment and localization
495 in the airways and parenchyma to achieving effective control of *Mtb*.
496 In recent studies, we proposed a role for AMs to localize from airways into the lung parenchyma
497 as an effector mechanism of protection upon *Mtb* infection (10). Consistent with this proposed
498 role for AMs in early *Mtb* control, our new results here demonstrate that during BCG
499 vaccination, AMs continue to be retained within the airways, while in BCG vaccinated hosts
500 which also received Z-DC transfer, AMs are activated rapidly (day 8) and migrate into the
501 parenchyma compartment. In sharp contrast, the AMs in BCG vaccinated mice take up to 20
502 days to undergo activation. Similarly, recruited macrophages in BCG vaccinated mice are
503 mostly located within the vasculature, while Z-DC transfer activates the RMs to migrate into the
504 airway. These responses appear to be mediated by signaling in epithelial cells as mice deficient
505 in NFκβ signaling in $CCSP^+$ epithelial cells abrogate AM accumulation, downstream activation
506 and accumulation of IL-17 producing Ag85B-specific $CD4^+$ T cells in the lung. Epithelial cells
507 respond to several external stimulus including IL-17 and IL-22 and activate NFκβ dependent
508 signaling pathways to produce chemokines and other chemotactic factors required to favor
509 other immune cell recruitment and transmigration into inflamed tissues (29, 53). Based on the
510 increased susceptibility of mice lacking NFκβ signaling in epithelial cells compartment, we
511 propose that epithelial cells play an important role in mediating transmigration and specific
512 localization of immune cells within lung parenchyma following being activated by IL-17 and/or
513 IL-22. Lung epithelial cells can produce chemokines such as CXCL9, 10, 11 (54) and 13 in
514 presence of various stimuli (19, 55). Our published data show that IL-17 and IL-22 cytokines are
515 inducers of chemokines following *Mtb* infection (8, 19, 25, 34, 45). Additionally, our published
516 data suggest an important role of the CXCL13/CXCR5 in organizing the iBALT structures which
517 help in rapid containment of the disease (19). Moreover, IL-17 cytokine is also involved in the
518 initial formation of the iBALT structures following *Mtb* infection in mice (26). Therefore, our

519 results show that innate activation of DCs results in activation of epithelial signaling in the lung
520 to amplify accumulation of $CD4^+$ T cells that localize within the airways and parenchyma to
521 induce *Mtb* killing of infected macrophages.
522 In conclusion, using a model of early complete *Mtb* control in BCG vaccinated hosts we show
523 that rapid and early clonal expansion of activated cytokine-producing $CD4^+$ T cells in the lung
524 airway and parenchyma compartment are critical for mediating complete and early vaccine-
525 induced protection in *Mtb*-infected mice. Importantly, these protections are driven by early
526 signaling events in the lung epithelial cells that provide the signals required for localization of
527 $CD4^+$ T cells within the parenchyma for activation of macrophages, formation of iBALT
528 structures and subsequent *Mtb* killing. Our studies support the emerging idea that Th1/Th17-like
529 activated $CD4^+$ T cells are associated with models of sterilizing protection in macaques (23), and
530 in vaccine-induced protection in human TB vaccines M72/AS01E trial (56). Understanding the
531 early immune parameters that mediate effective and early *Mtb* control as demonstrated in this
532 study will shed novel insights into the mechanisms by which vaccine-induced $CD4^+$ T cells can
533 be enhanced to mediate complete control of *Mtb*.
534

535 **Materials and Methods**

536 **Mice**

537 C57BL/6 (B6), B6.129P2-Il10tm1Cgn/J ($Il10^{-/-}$), B6.129S2(C)-Itgaetm1Cmp/J (*Itgae*$^{-/-}$ or *Cd103*$^{-/-}$
538) mice were obtained from Jackson Laboratory (Bar Harbor, ME) and bred at Washington
539 University in St. Louis. Cryopreserved sperm from *Ccr8*$^{-/-}$ mice were generously donated by Dr.
540 Gwendalyn Randolph from Washington University in St. Louis and the in vitro fertilization was
541 done in the Micro-injection Core at Washington University in St Louis. *Ikk*$^{fl/fl}$ *Sftp*^{cre} mice were a
542 kind gift from Dr. Pasparakis (University of Cologne). $Il\text{-}22^{-/-(28)}$ and *Il-17*$^{-/-(57)}$ single knock outs
543 were crossed and bred at Washington University in St. Louis to generate *Il-17/Il22*$^{-/-}$. Mice were
544 age and sex-matched and used between 6-8 weeks of age. All mice were used and housed in

accordance with the National Institute of Health guidelines for housing and care of laboratory animals. All the experiments in this study were granted by the Washington University in St Louis Institutional Animal Care and Use Committee under protocol 20160129.

IFN-γ in vivo neutralization

300μg/ml of anti-IFN-γ blocking antibody (Clone XMG1.2, BioXcell) was administered intraperitoneally every other day starting at 8 dpi until the harvest at 20 dpi.

Bacterial infection and vaccination

M. bovis Bacille Calmette–Guerin (BCG Pasteur, Source: Trudeau Institute) and *Mtb* W. Beijing strain, HN878 (BEI Resources) were grown to mid-log phase in Proskauer Beck medium containing 0.05% Tween 80 and frozen in at -80º C. Mice were vaccinated with 1 X 10^6 colony forming units (CFU) BCG subcutaneous and 4 weeks later infected with ~100 CFU *Mtb* HN878 via aerosol route using a Glas-Col airborne infection system. At given time points following infection, lungs were collected, homogenized and the tissue homogenates were plated following serial dilutions on 7H11 agar (BD bioscience) to assess bacterial burden (8).

In vitro culture of BMDCs and transfer

Bone marrow-derived dendritic cells (BMDC) and bone marrow-derived macrophages (BMDMs) were generated as previously described (8). Briefly, cells isolated from the femur and tibia were cultured at 1 X 10^6 cells/ml in 10 ml of complete DMEM (cDMEM) supplemented with 4% recombinant mouse GM-CSF (Peprotech, Rocky Hill, NJ, USA) at 37°C in 7.5% CO_2. After 3 days, 10 ml of cDMEM supplemented with 4% mouse GM-CSF was added and incubation continued till day 7. At day 7, non-adherent cells (BMDCs) were collected, counted, plated at 2 X 10^6 cells/ml in cDMEM and rested overnight at 37°C in 7.5% CO_2 following which BMDCs were stimulated overnight with Ag85B (20 μg/ml) (New England Peptide) and Zymosan (25 μg/ml) (Sigma) to induce maturation and activation. Mature pulsed BMDCs were collected,

569 washed and 1 X 10^6 cells in 50 ul PBS were instilled via intratracheal (IT) route at -1 and +4 dpi.
570 For all the adoptive transfer of Z-DCs, $Il10^{-/-}$ BMDC were used.

571 **Generation of single-cell suspensions from tissues**

572 Lung single-cell suspensions from vaccinated or *Mtb*-infected mice were isolated as previously
573 described (58). Briefly, mice were euthanized with CO_2 and lungs were perfused with heparin in
574 saline. Lungs were minced and incubated in Collagenase/DNAse for 30 minutes at 37°C. Lung
575 tissue was pushed through a 70 µm nylon screen to obtain a single cell suspension. Red blood
576 cells were lysed and the cells were resuspended in suitable media or buffer for further use.

577 **$CD4^+$ T cell isolation for RNA sequencing and adoptive transfer**

578 Single cells suspensions from infected mice were obtained as before (8). $CD4^+$ T cells from
579 differently treated mice were isolated using $CD4^+$ microbeads according to manufacturer's
580 instruction (Miltenyi Biotec). The purity of $CD4^+$ T cells was analyzed by flow cytometry after the
581 staining with anti-CD4 antibody and reported to be > 95%. For the RNA sequencing analysis,
582 cells were collected in RLT buffer with β-mercaptoethanol and processed according the
583 manufacturer's instructions (Qiagen). For T cell transfer, 2 X 10^6 $CD4^+$ T cells were transferred
584 via IT route in PBS into each mouse as previously described.

585 **RNA-Seq data analysis**

586 Purified mouse lung $CD4^+$ T cells were snap-frozen in RLT buffer, and DNase-treated total RNA
587 was extracted using the Qiagen RNeasy Mini kit (Qiagen). RNA-seq libraries were generated
588 using the Clontech SMART-Seq v4 Ultra Low Input RNA Kit for sequencing and the Illumina
589 Nextera XT DNA Library preparation kit following the manufacturer's protocol. Raw sequencing
590 reads were quality checked for potential sequencing issues and contaminants using FastQC.
591 Adapter sequences, primers, Ns, and reads with quality score below 28 were trimmed using
592 fastq-mcf of ea-utils and PRINSEQ. Reads with a remaining length of less than 20bp after
593 trimming were discarded. Paired end reads were mapped to the mouse genome (mm10) using
594 STAR in a strand specific manner. Read coverage on forward and reverse strands for genome

595 browser visualization was computed using SAMtools, BEDtools, and UCSC Genome Browser
596 utilities. Pairwise differential expression was quantified using DESeq2 (version 1.24.0), with
597 default settings and a 10-5 adjusted P value cutoff for significance, and DESeq2-normalized
598 read counts were used to calculate relative expression (FPKM) values. Heatmap figures were
599 generated in Microsoft Excel, using Z-scores calculated from the FPKM values across all of the
600 samples, individually for each gene. ”Principal Components Analysis (PCA) was performed
601 according to default DESeq2 settings, utilizing the top 500 most variable genes across all
602 samples. Lists of significantly differentially expressed genes were used to test for significant
603 enrichment among KEGG pathways(59) using WebGestalt(60) (default settings, adjusted P =
604 0.05 threshold for enrichment).

605 **scRNA-Seq library generation and sequencing**
606
607 Isolated total lung single cell suspensions were enriched for live cells using dead cell depletion
608 kit according to manufacturer’s instruction (Milteny Biotec) and subjected to droplet-based
609 massively parallel single-cell RNA sequencing using Chromium Single Cell 5’ (v3) Reagent Kit
610 as per manufacturer’s instructions (10x Genomics). Briefly, cell suspensions were loaded at
611 1,000 cells/µL with the aim to capture 10,000 cells/lane. The 10x Chromium Controller
612 generated GEM droplets, where each cell was labeled with a specific barcode, and each
613 transcript labeled with a unique molecular identifier (UMI) during reverse transcription. The
614 barcoded cDNA was isolated and removed from the BSL-3 space for library generation. The
615 cDNA underwent 11 cycles of amplification, followed by fragmentation, end repair, A-tailing,
616 adapter ligation, and sample index PCR as per the manufacturer’s instructions. Libraries were
617 sequenced on a NovaSeq S4 (200 cycle) flow cell, targeting 50,000 read pairs/cell.

618 **scRNA-Seq analysis**

619 Sample demultiplexing, barcode processing, and single-cell 5’ counting was performed using
620 the Cell Ranger Single-Cell Software Suite (10x Genomics, version 3). Cell ranger cell count
621 was used to align samples to the reference mm10 genome, quantify and filter reads with a

quality score below 30. For TCR, the Seurat package (61) in R was used for subsequent analysis. Cells with mitochondrial content greater than 10% were removed. Filtered data were normalized using a scaling factor of 10,000 nUMI was regressed with a negative binomial model, and data was log transformed. The highly variable genes were selected using the FindVariableFeatures. The principal component analysis was performed using the top 3000 variable genes. Clustering was performed using the FindClusters function. UMAP was used to project cells into two dimensions using 15 first principal components. For T cell re-clustering we chose clusters that were identified as T cells ($Cd3d^+$). For these 24758 cells we performed normalization, found variable genes and performed PCA, UMAP and clustering as described above. All visualization was done with ggplot2 R package (62), heatmaps were done with Phantasus website (https://artyomovlab.wustl.edu/phantasus/).

Public bulk RNA-seq reanalysis: We re-analyzed the publicly available GSE94964 dataset. With Phantasus, we filtered low expressed genes and did log2(exp+1) and quantile normalization. Further, to get the T resident memory signature for $CD4^+$ T cells, we compared $CD4^+$ $CD69^+$ samples from the lung with $CD4^+CD69^-$ samples from the lung and blood with limma. We have taken 500 upregulated genes. To compare with effector CD4_1 cluster from our data, we run FindMarkers function for CD4_1 cluster versus CD4_2 and CD4 Naïve cells with “MAST” algorithm, logFC threshold of 0.15 and “min.pct” parameter of 0.2. We used the resulted ranked gene list and 500 upregulated genes from the GSE94964 dataset as a signature to run GSEA with the fgsea package.

Single cell paired TCRα/TCRβ repertoire analysis

Sample demultiplexing and barcode processing was performed using the Cell Ranger Single-Cell Software Suite (10x Genomics). Cell Ranger VDJ v3 was used to align reads to the reference genome (vdj_GRCm38_alts_ensembl) and assemble TCRs. For downstream analysis, only TCRs with 1 productive rearrangement for TCRα chain and 1 productive

rearrangement for TCRβ chain were selected. Frequencies of clonotypes were calculated based on number of cells that pass quality control as described above and share both TCRα and TCRβ nucleotide sequences. Gini coefficient was computed with "gini" function from TCR R package. To infer motifs, TCRdist tool was used (63) on all TCRs that satisfied two criteria: that they belonged to CD4 T cells and that they had exactly 1 TCRβ and 1 TCRα chain with CDR3 sequence that passed cellranger quality control. TCRdist was run with default settings for "mouse" organism. We chose three motifs that were most abundant among unique clonotypes, without accounting for clonotype expansion. To characterize the motif and match it to TCRs, we have chosen the most conservative stretches amino acids to represent each motif: "NTGKL" in TCRα and "SLE" in TCRβ for motif 1, "NNNNAP" in TCRα and "E[TR]L" for motif 2, and "NAYKV" in TCRα and "SLE" in TCRβ for motif 3. All clonotypes that contained these sequences were classified as motif-bearing clonotypes. To calculate frequencies of cells for motifs, we calculated how many cells are having motif-bearing TCR clonotype. Further, motif-bearing TCRs were used to visualize motifs by first performing multiple sequence alignment with the msa R package (ClustalW algorithm), and after representing the motifs with the ggseqlogo R package.

Intratracheal and intravascular staining

Mice were anesthetized with Isoflurane before the IT and IV staining. For IT staining, 0.7 µg/mouse of anti-CD45.2-v500 ab (clone 104, BD Biosciences) in 50 ul of PBS was instilled through intratracheal route 15 minutes before the harvest. For the IV staining, 2.5 µg/mouse of anti-CD45.2-BV605 ab (clone 104, BD) in 100 ul of PBS were injected into the retro-orbital sinus 3 minutes before the harvest using a 26-gauge needle and a tuberculin syringe (10).

Flow cytometry staining

The following antibodies were from TonBo Biosciences: MHC-II (clone M5/114.15.2), IFN-γ (clone XMG1.2) and CD4 (clone RM4-5). Antibodies purchased from eBioscience (San Diego,

CA, USA) were: CD103 (clone 2E7), CD44 (clone IM7) and CXCR3 (clone CXCR3-173). CD11b (clone M1/70), CD11c (clone HL3), Gr1 (clone RB6-8C5), SIGLEC-F (clone E50-2440), CD3 (clone 500A2), CD4 (clone RM4-5) and IL-17 (clone TC11-18H10) were purchased from BD Biosciences. Ag85B tetramers were obtained from NIH tetramer core. For flow cytometric analysis, lung single cell suspensions were stained with tetramer prior to the surface and intracellular staining for 1 hour at 37°C.Intracellular cytokine staining was performed using the BD Cytofix/Cytoperm kit (BD Biosciences) following manufacturer's instructions. Intracellular staining with anti-IFN-γ and IL-17 was performed for 30 minutes. Cells single stained with each fluorochrome were used as controls for the compensation matrix in the flow cytometry. Samples were acquired on a 4 laser BD Fortessa Flow Cytometer and the analysis was performed using FlowJo (Treestar).

Immunofluorescence staining

For immunofluorescent staining, formalin fixed and paraffin embedded (FFPE) lung sections were cut, immersed in xylene, and then hydrated in 96% alcohol and phosphate-buffered saline. Antigens were unmasked using a DakoCytomation Target Retrieval Solution (Dako), and non-specific binding was blocked by adding 5% (v/v) normal donkey serum and Fc block (BD). Avidin was used to neutralize endogenous biotin, followed by incubation with biotin (Sigma Aldrich). Sections were then probed with anti-B220 (clone RA3-6B2, BD) and anti-CD3 (clone M-20, Santa Cruz Biotechnology) to detect B cells and T cells respectively. For analysis of B-cell follicles, follicles were outlined with an automated tool of the Zeiss Axioplan 2 microscope (Zeiss), and total area and average size was calculated in squared microns.

Cytokine and chemokine quantification using Luminex or ELISA

Cytokine and chemokine protein contents in lung homogenates were quantified using Luminex multianalyte technology (Millipore) according to manufacturer’s protocols. IL-17, IFN-γ was quantified by ELISA according to manufacturer’s instructions (R&D).

Statistical Analysis

The differences between two groups were analyzed using two-tailed student's t test in Prism 5 (GraphPad). Differences between the means of three or more groups were analyzed using One-way ANOVA with Tukey's post-test. For comparisons between two or more groups with two independent variables, 2-way ANOVA with Sidak's or Tukey's post-test was used. A p-value of <0.05 was considered significant. Raw read counts were used as input for DESeq2(64) (version 1.24.0) differential expression analysis, using default settings and an FDR-adjusted P value threshold of 10^{-5} for significant differential expression. Lists of significantly differentially expressed genes were used to test for significant enrichment among KEGG pathways (59) using WebGestalt (60) (default settings, adjusted P = 0.05 threshold for enrichment).

Data availability statement

scRNA-Seq data that support the findings of this study have been deposited in GEO (ID GSE150657) and synapse (ID syn22036882). RNA-Seq data that support the findings of this study have been deposited in GEO (accession number: GSE165614). Other data that support the findings of this study are available from the corresponding author upon request.

Declaration of interest

The authors declare no competing interests.

Acknowledgement

This work was supported by Washington University School of Medicine, NIH grant HL105427, AI111914-02, AI134236-02 and AI123780 to S.A.K. and D.K., the Department of Molecular Microbiology, Washington University School of Medicine, and Stephen I. Morse Fellowship to S.D. J.R.-M. was supported by funds of the Department of Medicine, University of Rochester, and NIH grant U19 AI91036. We thank the Genome Engineering and iPSC Center and Department of Pathology Micro-Injection Core (Washington University School of Medicine) for assistance in generating the *Ccr8*$^{-/-}$ mice, NIH tetramer core facility for generously providing

Ag85B tetramers and Ms. Lan Lu and Ms. Misty Veschak (Washington University School of Medicine) for technical support.

Author contributions

S.A.K. designed the study, provided funding. S.D., N.D.M., and M.A. performed mouse experiments and compiled the results. E.E., A.S., M.N.A, B.A.R., and M.M. performed the scRNA-Seq and RNA-Seq analysis, comparative transcriptomics, and functional enrichment analysis. J.R.-M. performed histochemical analysis. M.G.N., L.B.B., M.Z., M.N.A., D.K., and S.A.K. interpreted experiments, carried out data analysis and/or provided reagents. S.A.K., S.D., and E.E wrote the manuscript, all authors edited and approved the final version of the manuscript.

References

1. **WHO.** 2018. Tuberculosis Fact sheet http://www.who.int/mediacentre/factsheets/fs104/en/. Accessed
2. **Tait DR, Hatherill M, Van Der Meeren O, Ginsberg AM, Van Brakel E, Salaun B, Scriba TJ, Akite EJ, Ayles HM, Bollaerts A, Demoitie MA, Diacon A, Evans TG, Gillard P, Hellstrom E, Innes JC, Lempicki M, Malahleha M, Martinson N, Mesia Vela D, Muyoyeta M, Nduba V, Pascal TG, Tameris M, Thienemann F, Wilkinson RJ, Roman F.** 2019. Final Analysis of a Trial of M72/AS01E Vaccine to Prevent Tuberculosis. N Engl J Med **381:**2429-2439.
3. **Darrah PA, Zeppa JJ, Maiello P, Hackney JA, Wadsworth MH, 2nd, Hughes TK, Pokkali S, Swanson PA, 2nd, Grant NL, Rodgers MA, Kamath M, Causgrove CM, Laddy DJ, Bonavia A, Casimiro D, Lin PL, Klein E, White AG, Scanga CA, Shalek AK, Roederer M, Flynn JL, Seder RA.** 2020. Prevention of tuberculosis in macaques after intravenous BCG immunization. Nature **577:**95-102.
4. **Kaushal D, Foreman TW, Gautam US, Alvarez X, Adekambi T, Rangel-Moreno J, Golden NA, Johnson AM, Phillips BL, Ahsan MH, Russell-Lodrigue KE, Doyle LA, Roy CJ, Didier PJ, Blanchard JL, Rengarajan J, Lackner AA, Khader SA, Mehra S.** 2015. Mucosal vaccination with attenuated Mycobacterium tuberculosis induces strong central memory responses and protects against tuberculosis. Nat Commun **6:**8533.
5. **Verreck FAW, Tchilian EZ, Vervenne RAW, Sombroek CC, Kondova I, Eissen OA, Sommandas V, van der Werff NM, Verschoor E, Braskamp G, Bakker J, Langermans JAM, Heidt PJ, Ottenhoff THM, van Kralingen KW, Thomas AW, Beverley PCL, Kocken CHM.** 2017. Variable BCG efficacy in rhesus populations: Pulmonary BCG provides protection where standard intra-dermal vaccination fails. Tuberculosis (Edinb) **104:**46-57.
6. **Caruso AM, Serbina N, Klein E, Triebold K, Bloom BR, Flynn JL.** 1999. Mice deficient in CD4 T cells have only transiently diminished levels of IFN-gamma, yet succumb to tuberculosis. J Immunol **162:**5407-5416.
7. **Urdahl KB, Shafiani S, Ernst JD.** 2011. Initiation and regulation of T-cell responses in tuberculosis. Mucosal immunology **4:**288-293.
8. **Griffiths KL, Ahmed M, Das S, Gopal R, Horne W, Connell TD, Moynihan KD, Kolls JK, Irvine DJ, Artyomov MN, Rangel-Moreno J, Khader SA.** 2016. Targeting dendritic cells to accelerate T-cell activation overcomes a bottleneck in tuberculosis vaccine efficacy. Nat Commun **7:**13894.
9. **Portal-Celhay C, Tufariello JM, Srivastava S, Zahra A, Klevorn T, Grace PS, Mehra A, Park HS, Ernst JD, Jacobs WR, Jr., Philips JA.** 2016. Mycobacterium tuberculosis EsxH inhibits ESCRT-dependent CD4(+) T-cell activation. Nat Microbiol **2:**16232.
10. **Dunlap MD, Howard N, Das S, Scott N, Ahmed M, Prince O, Rangel-Moreno J, Rosa BA, Martin J, Kaushal D, Kaplan G, Mitreva M, Kim KW, Randolph GJ, Khader SA.** 2018. A novel role for C-C motif chemokine receptor 2 during infection with hypervirulent Mycobacterium tuberculosis. Mucosal Immunol **11:**1727-1742.
11. **Sakai S, Kauffman KD, Schenkel JM, McBerry CC, Mayer-Barber KD, Masopust D, Barber DL.** 2014. Cutting edge: control of Mycobacterium tuberculosis infection by a subset of lung parenchyma-homing CD4 T cells. J Immunol **192:**2965-2969.
12. **Khader SA, Bell GK, Pearl JE, Fountain JJ, Rangel-Moreno J, Cilley GE, Shen F, Eaton SM, Gaffen SL, Swain SL, Locksley RM, Haynes L, Randall TD, Cooper AM.** 2007. IL-23 and IL-17 in the establishment of protective pulmonary CD4+ T cell responses after vaccination and during Mycobacterium tuberculosis challenge. Nat Immunol **8:**369-377.
13. **Ogongo P, Porterfield JZ, Leslie A.** 2019. Lung Tissue Resident Memory T-Cells in the Immune Response to Mycobacterium tuberculosis. Front Immunol **10:**992.

14. **Kumar BV, Ma W, Miron M, Granot T, Guyer RS, Carpenter DJ, Senda T, Sun X, Ho SH, Lerner H, Friedman AL, Shen Y, Farber DL.** 2017. Human Tissue-Resident Memory T Cells Are Defined by Core Transcriptional and Functional Signatures in Lymphoid and Mucosal Sites. Cell Rep **20:**2921-2934.
15. **Karlsson AK, Walles K, Bladh H, Connolly S, Skrinjar M, Rosendahl A.** 2011. Small molecule antagonists of CCR8 inhibit eosinophil and T cell migration. Biochem Biophys Res Commun **407:**764-771.
16. **Mami-Chouaib F, Blanc C, Corgnac S, Hans S, Malenica I, Granier C, Tihy I, Tartour E.** 2018. Resident memory T cells, critical components in tumor immunology. J Immunother Cancer **6:**87.
17. **Hara-Chikuma M, Chikuma S, Sugiyama Y, Kabashima K, Verkman AS, Inoue S, Miyachi Y.** 2012. Chemokine-dependent T cell migration requires aquaporin-3-mediated hydrogen peroxide uptake. J Exp Med **209:**1743-1752.
18. **Lai EC.** 2004. Notch signaling: control of cell communication and cell fate. Development **131:**965-973.
19. **Slight SR, Rangel-Moreno J, Gopal R, Lin Y, Fallert Junecko BA, Mehra S, Selman M, Becerril-Villanueva E, Baquera-Heredia J, Pavon L, Kaushal D, Reinhart TA, Randall TD, Khader SA.** 2013. CXCR5+ T helper cells mediate protective immunity against tuberculosis. J Clin Invest **123:**712-726.
20. **Lindenstrom T, Moguche A, Damborg M, Agger EM, Urdahl K, Andersen P.** 2018. T Cells Primed by Live Mycobacteria Versus a Tuberculosis Subunit Vaccine Exhibit Distinct Functional Properties. EBioMedicine **27:**27-39.
21. **Sallin MA, Sakai S, Kauffman KD, Young HA, Zhu J, Barber DL.** 2017. Th1 Differentiation Drives the Accumulation of Intravascular, Non-protective CD4 T Cells during Tuberculosis. Cell Rep **18:**3091-3104.
22. **Gopal R, Monin L, Slight S, Uche U, Blanchard E, Fallert Junecko BA, Ramos-Payan R, Stallings CL, Reinhart TA, Kolls JK, Kaushal D, Nagarajan U, Rangel-Moreno J, Khader SA.** 2014. Unexpected role for IL-17 in protective immunity against hypervirulent Mycobacterium tuberculosis HN878 infection. PLoS Pathog **10:**e1004099.
23. **Dijkman K, Sombroek CC, Vervenne RAW, Hofman SO, Boot C, Remarque EJ, Kocken CHM, Ottenhoff THM, Kondova I, Khayum MA, Haanstra KG.** 2019. Prevention of tuberculosis infection and disease by local BCG in repeatedly exposed rhesus macaques. **25:**255-262.
24. **McAllister F, Henry A, Kreindler JL, Dubin PJ, Ulrich L, Steele C, Finder JD, Pilewski JM, Carreno BM, Goldman SJ, Pirhonen J, Kolls JK.** 2005. Role of IL-17A, IL-17F, and the IL-17 receptor in regulating growth-related oncogene-alpha and granulocyte colony-stimulating factor in bronchial epithelium: implications for airway inflammation in cystic fibrosis. J Immunol **175:**404-412.
25. **Khader SA, Guglani L, Rangel-Moreno J, Gopal R, Junecko BA, Fountain JJ, Martino C, Pearl JE, Tighe M, Lin YY, Slight S, Kolls JK, Reinhart TA, Randall TD, Cooper AM.** 2011. IL-23 is required for long-term control of Mycobacterium tuberculosis and B cell follicle formation in the infected lung. J Immunol **187:**5402-5407.
26. **Rangel-Moreno J, Carragher DM, de la Luz Garcia-Hernandez M, Hwang JY, Kusser K, Hartson L, Kolls JK, Khader SA, Randall TD.** 2011. The development of inducible bronchus-associated lymphoid tissue depends on IL-17. Nat Immunol **12:**639-646.
27. **Kulkarni N, Pathak M, Lal G.** 2017. Role of chemokine receptors and intestinal epithelial cells in the mucosal inflammation and tolerance. J Leukoc Biol **101:**377-394.
28. **Treerat P, Prince O, Cruz-Lagunas A, Munoz-Torrico M, Salazar-Lezama MA, Selman M, Fallert-Junecko B, Reinhardt TA, Alcorn JF, Kaushal D, Zuniga J, Rangel-Moreno J, Kolls JK, Khader SA.**

2017. Novel role for IL-22 in protection during chronic Mycobacterium tuberculosis HN878 infection. Mucosal Immunol **10:**1069-1081.

29. **Hernandez-Santos N, Wiesner DL, Fites JS, McDermott AJ, Warner T, Wuthrich M, Klein BS.** 2018. Lung Epithelial Cells Coordinate Innate Lymphocytes and Immunity against Pulmonary Fungal Infection. Cell Host Microbe **23:**511-522.e515.
30. **Perez-Nazario N, Rangel-Moreno J, O'Reilly MA, Pasparakis M, Gigliotti F, Wright TW.** 2013. Selective ablation of lung epithelial IKK2 impairs pulmonary Th17 responses and delays the clearance of Pneumocystis. J Immunol **191:**4720-4730.
31. **Harding CV, Boom WH.** 2010. Regulation of antigen presentation by Mycobacterium tuberculosis: a role for Toll-like receptors. Nat Rev Microbiol **8:**296-307.
32. **Carpenter SM, Yang JD.** 2017. Vaccine-elicited memory CD4+ T cell expansion is impaired in the lungs during tuberculosis. **13:**e1006704.
33. **Hope JC, Kwong LS, Sopp P, Collins RA, Howard CJ.** 2000. Dendritic cells induce CD4+ and CD8+ T-cell responses to Mycobacterium bovis and M. avium antigens in Bacille Calmette Guérin vaccinated and nonvaccinated cattle. Scand J Immunol **52:**285-291.
34. **Gopal R, Lin Y, Obermajer N, Slight S, Nuthalapati N, Ahmed M, Kalinski P, Khader SA.** 2012. IL-23-dependent IL-17 drives Th1-cell responses following Mycobacterium bovis BCG vaccination. Eur J Immunol **42:**364-373.
35. **Moguche AO, Musvosvi M, Penn-Nicholson A, Plumlee CR, Mearns H, Geldenhuys H, Smit E, Abrahams D, Rozot V, Dintwe O, Hoff ST, Kromann I, Ruhwald M, Bang P, Larson RP, Shafiani S, Ma S, Sherman DR, Sette A, Lindestam Arlehamn CS, McKinney DM, Maecker H, Hanekom WA, Hatherill M, Andersen P, Scriba TJ, Urdahl KB.** 2017. Antigen Availability Shapes T Cell Differentiation and Function during Tuberculosis. Cell Host Microbe **21:**695-706.e695.
36. **Lin PL, Dietrich J, Tan E, Abalos RM, Burgos J, Bigbee C, Bigbee M, Milk L, Gideon HP, Rodgers M, Cochran C, Guinn KM, Sherman DR, Klein E, Janssen C, Flynn JL, Andersen P.** 2012. The multistage vaccine H56 boosts the effects of BCG to protect cynomolgus macaques against active tuberculosis and reactivation of latent Mycobacterium tuberculosis infection. J Clin Invest **122:**303-314.
37. **Woodworth JS, Cohen SB, Moguche AO, Plumlee CR, Agger EM, Urdahl KB, Andersen P.** 2017. Subunit vaccine H56/CAF01 induces a population of circulating CD4 T cells that traffic into the Mycobacterium tuberculosis-infected lung. Mucosal Immunol **10:**555-564.
38. **Carpenter SM, Yang JD, Lee J, Barreira-Silva P, Behar SM.** 2017. Vaccine-elicited memory CD4+ T cell expansion is impaired in the lungs during tuberculosis. PLoS Pathog **13:**e1006704.
39. **Srivastava S, Ernst JD.** 2013. Cutting edge: Direct recognition of infected cells by CD4 T cells is required for control of intracellular Mycobacterium tuberculosis in vivo. J Immunol **191:**1016-1020.
40. **Saha PK, Sharma PK, Sharma SK, Singh A, Mitra DK.** 2013. Recruitment of Th1 effector cells in human tuberculosis: hierarchy of chemokine receptor(s) and their ligands. Cytokine **63:**43-51.
41. **Perreau M, Rozot V, Welles HC, Belluti-Enders F, Vigano S, Maillard M, Dorta G, Mazza-Stalder J, Bart PA, Roger T, Calandra T, Nicod L, Harari A.** 2013. Lack of Mycobacterium tuberculosis-specific interleukin-17A-producing CD4+ T cells in active disease. Eur J Immunol **43:**939-948.
42. **Lindestam Arlehamn CS, Gerasimova A, Mele F, Henderson R, Swann J, Greenbaum JA, Kim Y, Sidney J, James EA, Taplitz R, McKinney DM, Kwok WW, Grey H, Sallusto F, Peters B, Sette A.** 2013. Memory T cells in latent Mycobacterium tuberculosis infection are directed against three antigenic islands and largely contained in a CXCR3+CCR6+ Th1 subset. PLoS Pathog **9:**e1003130.
43. **Shanmugasundaram U, Bucsan AN, Ganatra SR, Ibegbu C, Quezada M, Blair RV, Alvarez X, Velu V, Kaushal D, Rengarajan J.** 2020. Pulmonary Mycobacterium tuberculosis control associates with CXCR3- and CCR6-expressing antigen-specific Th1 and Th17 cell recruitment. JCI Insight **5**.

44. **Gopal R, Monin L, Torres D, Slight S, Mehra S, McKenna KC, Fallert Junecko BA, Reinhart TA, Kolls J, Baez-Saldana R, Cruz-Lagunas A, Rodriguez-Reyna TS, Kumar NP, Tessier P, Roth J, Selman M, Becerril-Villanueva E, Baquera-Heredia J, Cumming B, Kasprowicz VO, Steyn AJ, Babu S, Kaushal D, Zuniga J, Vogl T, Rangel-Moreno J, Khader SA.** 2013. S100A8/A9 proteins mediate neutrophilic inflammation and lung pathology during tuberculosis. Am J Respir Crit Care Med **188:**1137-1146.

45. **Kumar P, Monin L, Castillo P, Elsegeiny W, Horne W, Eddens T, Vikram A, Good M, Schoenborn AA, Bibby K, Montelaro RC, Metzger DW, Gulati AS, Kolls JK.** 2016. Intestinal Interleukin-17 Receptor Signaling Mediates Reciprocal Control of the Gut Microbiota and Autoimmune Inflammation. Immunity **44:**659-671.

46. **Cepek KL, Shaw SK, Parker CM, Russell GJ, Morrow JS, Rimm DL, Brenner MB.** 1994. Adhesion between epithelial cells and T lymphocytes mediated by E-cadherin and the alpha E beta 7 integrin. Nature **372:**190-193.

47. **Perdomo C, Zedler U, Kuhl AA, Lozza L, Saikali P, Sander LE, Vogelzang A, Kaufmann SH, Kupz A.** 2016. Mucosal BCG Vaccination Induces Protective Lung-Resident Memory T Cell Populations against Tuberculosis. MBio **7**.

48. **Copland A, Diogo GR, Hart P, Harris S, Tran AC, Paul MJ, Singh M, Cutting SM, Reljic R.** 2018. Mucosal Delivery of Fusion Proteins with Bacillus subtilis Spores Enhances Protection against Tuberculosis by Bacillus Calmette-Guérin. Front Immunol **9:**346.

49. **Schön MP, Arya A, Murphy EA, Adams CM, Strauch UG, Agace WW, Marsal J, Donohue JP, Her H, Beier DR, Olson S, Lefrancois L, Brenner MB, Grusby MJ, Parker CM.** 1999. Mucosal T lymphocyte numbers are selectively reduced in integrin alpha E (CD103)-deficient mice. J Immunol **162:**6641-6649.

50. **Soler D, Chapman TR, Poisson LR, Wang L, Cote-Sierra J, Ryan M, McDonald A, Badola S, Fedyk E, Coyle AJ, Hodge MR, Kolbeck R.** 2006. CCR8 expression identifies CD4 memory T cells enriched for FOXP3+ regulatory and Th2 effector lymphocytes. J Immunol **177:**6940-6951.

51. **Thuong NT, Dunstan SJ, Chau TT, Thorsson V, Simmons CP, Quyen NT, Thwaites GE, Thi Ngoc Lan N, Hibberd M, Teo YY, Seielstad M, Aderem A, Farrar JJ, Hawn TR.** 2008. Identification of tuberculosis susceptibility genes with human macrophage gene expression profiles. PLoS Pathog **4:**e1000229.

52. **Blischak JD, Tailleux L, Myrthil M, Charlois C, Bergot E, Dinh A, Morizot G, Chény O, Platen CV, Herrmann JL.** 2017. Predicting susceptibility to tuberculosis based on gene expression profiling in dendritic cells. **7:**5702.

53. **Tully JE, Nolin JD, Guala AS, Hoffman SM, Roberson EC, Lahue KG, van der Velden J, Anathy V, Blackwell TS, Janssen-Heininger YM.** 2012. Cooperation between classical and alternative NF-κB pathways regulates proinflammatory responses in epithelial cells. Am J Respir Cell Mol Biol **47:**497-508.

54. **Sauty A, Dziejman M, Taha RA, Iarossi AS, Neote K, Garcia-Zepeda EA, Hamid Q, Luster AD.** 1999. The T cell-specific CXC chemokines IP-10, Mig, and I-TAC are expressed by activated human bronchial epithelial cells. J Immunol **162:**3549-3558.

55. **Wang GZ, Cheng X, Zhou B, Wen ZS, Huang YC, Chen HB, Li GF, Huang ZL, Zhou YC, Feng L, Wei MM, Qu LW, Cao Y, Zhou GB.** 2015. The chemokine CXCL13 in lung cancers associated with environmental polycyclic aromatic hydrocarbons pollution. Elife **4**.

56. **Sable SB, Posey JE, Scriba TJ.** 2019. Tuberculosis Vaccine Development: Progress in Clinical Evaluation. Clin Microbiol Rev **33**.

57. **Gopal R, Monin L, Slight S, Uche U, Blanchard E, Fallert Junecko BA, Ramos-Payan R, Stallings CL, Reinhart TA, Kolls JK, Kaushal D, Nagarajan U, Rangel-Moreno J, Khader SA.** 2014.

Unexpected role for IL-17 in protective immunity against hypervirulent Mycobacterium tuberculosis HN878 infection.

58. **Ardain A, Domingo-Gonzalez R, Das S, Kazer SW, Howard NC, Singh A, Ahmed M, Nhamoyebonde S, Rangel-Moreno J, Ogongo P, Lu L, Ramsuran D, de la Luz Garcia-Hernandez M, T KU, Darby M, Park E, Karim F, Melocchi L, Madansein R, Dullabh KJ, Dunlap M, Marin-Agudelo N, Ebihara T, Ndung'u T, Kaushal D, Pym AS, Kolls JK, Steyn A, Zuniga J, Horsnell W, Yokoyama WM, Shalek AK, Kloverpris HN, Colonna M, Leslie A, Khader SA.** 2019. Group 3 innate lymphoid cells mediate early protective immunity against tuberculosis. Nature **570:**528-532.

59. **Kanehisa M, Sato Y, Furumichi M, Morishima K, Tanabe M.** 2019. New approach for understanding genome variations in KEGG. Nucleic Acids Res **47:**D590-d595.

60. **Liao Y, Wang J, Jaehnig EJ, Shi Z, Zhang B.** 2019. WebGestalt 2019: gene set analysis toolkit with revamped UIs and APIs. Nucleic Acids Res **47:**W199-w205.

61. **Butler A, Hoffman P, Smibert P, Papalexi E, Satija R.** 2018. Integrating single-cell transcriptomic data across different conditions, technologies, and species. Nat Biotechnol **36:**411-420.

62. **Wickham H.** 2016. ggplot2: Elegant Graphics for Data Analysis. Springer-Verlag New York.

63. **Dash P, Fiore-Gartland AJ, Hertz T, Wang GC, Sharma S, Souquette A, Crawford JC, Clemens EB, Nguyen THO, Kedzierska K, La Gruta NL, Bradley P, Thomas PG.** 2017. Quantifiable predictive features define epitope-specific T cell receptor repertoires. Nature **547:**89-93.

64. **Love MI, Huber W, Anders S.** 2014. Moderated estimation of fold change and dispersion for RNA-seq data with DESeq2. Genome Biol **15:**550.

957 **Figure Legends:**

958 **Figure 1. Activation of DCs amplifies rapid CD4$^+$ T cell responses in BCG vaccinated *Mtb***
959 **infected mice.** C57BL/6 (B6) mice were either left unvaccinated (UnVac) or vaccinated with
960 BCG (Vac), rested for 4 weeks and infected with *Mtb* HN878. Some BCG vaccinated mice
961 received Z-DC (Vac+Z-DC) at the time of *Mtb* infection (A). Lungs were harvested at different
962 dpi and single cell suspensions were subjected to scRNA-Seq. UMAP with lung isolated CD3$^+$
963 cells, combined plot shown from unvaccinated (20 dpi) (n=2), vaccinated (15 dpi) (n=2), Vac+Z-
964 DC (8 and 15 dpi) (n=1 and n=2 respectively) conditions are presented here (**B**). UMAPs with
965 marker genes used to assign identity to clusters of T cells are shown (**C**). CD4$^+$ cluster
966 abundances as percent of total CD3$^+$ cells across four conditions are shown. Error bars are
967 mean $\pm$ SD for two replicates from each condition. Vac+Z-DC 8 dpi had only one replicate (**D**).
968 Mean expression of genes, upregulated (left panel) or downregulated (right panel) in lung T
969 resident memory (Trm) cells on UMAP for all conditions are shown (**E**). Gini coefficient for CD4$^+$
970 repertoires across all samples are shown (**F**). TCRdist tree result for 7677 unique CD4$^+$ TCRs
971 are shown (**G**). Amino acid composition of CDR3α and CDR3β for motif 1 depicted as sequence
972 logo (**H**). Proportion of CD4$^+$ cells, matching motif 1 across all samples (left panel) and across
973 CD4$^+$ clusters (right panel) are shown (**I**). Gene expression profile of total CD4$^+$ T cells isolated
974 from *Mtb*-infected unvaccinated (20 dpi), *Mtb*-infected BCG vaccinated (15 dpi), and *Mtb*-
975 infected BCG vaccinated C57BL/6 mice that receive Z-DC transfer (8 dpi), was determined by
976 RNA sequencing **(J).** Z-scores calculated from the FPKM values across all of the samples,
977 individually for each gene. n = 5 biological replicates for gene expression profile analysis.

978 **Figure 2. Adoptive transfer of vaccine-induced CD4$^+$ T cells mediates improved *Mtb***
979 **control in BCG vaccinated host.** CD4$^+$ T cells were isolated from *Mtb*-infected BCG
980 vaccinated C57BL/6 mice and *Mtb*-infected BCG vaccinated C57BL/6 mice that received Z-DC
981 transfer and co-cultured with *Mtb*-infected BMDMs (1:1 ratio) for six days. Intracellular *Mtb* CFU
982 was determined by plating cell lysates **(A)**. IFN-γ and IL-17 levels **(B, C)** were measured in cell

supernatants by ELISA. n = 3-5 biological replicates. C57BL/6 mice were vaccinated with BCG, rested for 4 weeks and infected with *Mtb* HN878. $CD4^+$ T cells were isolated from *Mtb*-infected BCG vaccinated mice that received Z-DC transfer (at 8 dpi) and adoptively transferred to *Mtb*-infected BCG vaccinated mice. Lungs were harvested at 30 dpi and lung bacterial burden was determined by plating **(D).** Lung inflammation was calculated in the H&E stained FFPE lung sections (**E**). B cell lymphoid follicle formation was determined on the FFPE lung sections by B220 (red) immunofluorescence staining (**F**). n = 3-9 mice per group. Levels of cytokines (**G**) and chemokines (**H)** in lung homogenates were quantified by multiplex. n = 5 biological replicates. Data represented as mean $\pm$ SD. ND = not detected. ** p≤ 0.01, *** p≤0.001 either by one way ANOVA (**A-C)** or by Student's t test (actual p values are shown) **(D-H)**.

Figure 3. Rapid and early $CD4^+$ T cell activation and localization within lung parenchyma and airway is driven by CCR8 engagement. C57BL/6 mice were vaccinated, *Mtb*-infected and received Z-DC transfer as described in method. At the time of harvest, the mice received anti-CD45.2-v500 (IT) and anti-CD45.2-BV605 (IV) antibodies as described in method. Lungs were harvested and subjected to flow cytometry to measure the number of $CD4^+CD44^{hi}TET^+$ (**A**) T cells. The distribution of $CD4^+CD44^{hi}TET^+$ (**B**), $CD4^+CD44^{hi}TET^+CXCR3^+$ (**C**), $CD4^+CD44^{hi}TET^+$cytokine$^+$ (**D, E**), $CD4^+CD44^{hi}TET^+CD103^+$ (**I**), $CD4^+CD44^{hi}TET^+CCR8^+$ (**J**) T cells in groups of BCG vaccinated mice were measured in lung airways (red bar), parenchyma (blue bar) and vasculature (green bar) regions by flow cytometry. n=4-5 mice per group. B6, and *IL-17/IL-22*$^{-/-}$ mice were vaccinated with BCG, rested for 4 weeks and infected with *Mtb* HN878 and received Z-DC. One group of BCG vaccinated *Mtb*-infected *IL-17/IL-22*$^{-/-}$ mice received IFN-γ neutralizing ab. Mice were harvested at 20 dpi and lung bacterial burden was determined by plating **(F)**. MHC-II MFI (mean fluorescent intensity-MFI) on AMs (**G**) and number of $CD4^+CD44^{hi}TET^+$ T cells **(H)** were assessed by flow cytometry on total lung single cell suspensions. n=4-5 mice per group. B6, and *Ccr8*$^{-/-}$ mice were vaccinated with BCG, rested for

4 weeks and infected with *Mtb* HN878. Some BCG vaccinated mice received Z-DC. Mice were harvested at 20 dpi and lung bacterial burden was determined by plating **(K)**. Frequency of $CD4^+CD44^{hi}TET^+$ T cells **(L)** were assessed by flow cytometry on total lung single cell suspensions. n=4-8 mice per group. Data represented as mean ± SD.* p≤0.05, ** p≤ 0.01, *** p≤ 0.001, ****p≤ 0.0001 either by two-way ANOVA (**A-E, I and J**), one-way ANOVA (**F-H**) or Student's t test (actual p values are shown) (**K and L**).

Figure 4. NFκβ signaling in lung epithelial cells mediates early $CD4^+$ T cell activation and mucosal localization. C57BL/6 mice were vaccinated, *Mtb*-infected and received Z-DCs as described in method. To track the myeloid cells, mice were given anti-CD45.2-v500 and anti-CD45.2-BV605 antibodies through IT and IV route respectively prior to harvest. Lungs were harvested at different dpi and total numbers of AMs **(A)**,MHC-II MFI (mean fluorescent intensity-MFI) on AMs **(B)**, RMs **(C)**, MHC-II MFI on RMs **(D)** in airways (red bar), parenchyma (blue bar) and vasculature (green bar) location were assessed by flow cytometry. n=4-5 mice per group. In a separate experiment, $Ikk^{fl/fl}$ and $Ikk^{fl/fl}Sftp^{cre}$ mice were vaccinated with BCG, infected and received Z-DCs as described under method. To track the immune cells, mice were given anti-CD45.2-v500 and anti-CD45.2-BV605 antibodies through IT and IV route respectively prior to harvest. Lungs were harvested at 20 dpi and lung bacterial burden was determined by plating **(E)**. B cell lymphoid follicles were determined by CD3 (red) and B220 (green) staining on FFPE lung sections by immunofluorescence staining (**F**). The total numbers of AMs **(G)**, RMs **(H),** $CD4^+CD44^{hi}TET^+$ (**I**), $CD4^+CD44^{hi}TET^+cytokine^+$ (**J, K)** T cells in the airways, parenchyma and vasculature location were determined by flow cytometry (red=$Ikk^{fl/fl}$, n=4-9; blue= $Ikk^{fl/fl}Sftp^{cre}$, n=4-8*)*. Data represented as mean ± SD.* p≤0.05, ** p≤ 0.01, *** p≤0.001, ****p≤ 0.0001 either by two way ANOVA (**A-D, G-K**) or by Student's t test (actual p values are shown) (**E and F**).

Supplementary Figure legends:

Supplementary Figure 1. Mucosal delivery of Z-DCs in *Mtb*-infected BCG vaccinated mice results in unique *Mtb* antigen specific CD4$^+$ T cell activation at the site of infection. UMAP with CD3$^+$ cells, split by condition is shown (**A**). T cell cluster abundances as percent of total CD3$^+$ cells across four conditions are shown (**B**). Error bars are mean ± SD for two replicates from each condition. Vac+Z-DC 8 dpi had only one sample. Gene set enrichment analysis (GSEA) shows an enrichment of genes, upregulated in lung Trm (GSE94964), in our comparison between CD4_1 and CD4_2/Naive CD4 cluster (C). Amino acid composition of CDR3α and CDR3β for motif 2 and 3 depicted as sequence logos (**D**). Proportion of CD4$^+$ cells, matching motif 1 across all samples and clusters are shown (**E**).

Supplementary figure 2. RNA-Seq reveals unique gene signatures in CD4$^+$ T cells isolated from *Mtb*-infected BCG vaccinated C57BL/6 mice that received Z-DC transfer. CD4$^+$ T cells were isolated from *Mtb*-infected unvaccinated (20 dpi), *Mtb*-infected BCG vaccinated (15 dpi) and *Mtb*-infected BCG vaccinated mice that received Z-DC transfer (8 dpi) and RNA was extracted. Principal component analysis showing genes differentially expressed by CD4$^+$ T cells isolated from differently treated mice **(A)**. Table showing top 25 genes differentially expressed in CD4$^+$ T by *Mtb*-infected BCG vaccinated mice that received Z-DC transfer cells as compared with *Mtb*-infected BCG vaccinated mice **(B)**. KEGG pathway analysis showing the gene signatures upregulated in CD4$^+$ T from by *Mtb*-infected BCG vaccinated mice that received Z-DC transfer cells as compared with *Mtb*-infected BCG vaccinated mice **(C)**. C57BL/6 mice were vaccinated, infected and received Z-DC as described in method. At the time of harvest, the mice were given both anti-CD45.2-v500 and anti-CD45.2-BV605 antibodies through IT and IV route respectively. Lungs were harvested and subjected to flow cytometry. Gating strategy is shown to detect lung T cells populations. T cells were characterized as CD3$^+$CD4$^+$CD44^{hi}Tetramer$^+$ (D). These Tetramer$^+$ cells were further gated based on CD45.2-v500 and CD45.2-BV605 staining. CD3$^+$CD4$^+$CD44^{hi}Tetramer$^+$CD45.2-v500$^+$CD45.2-BV605$^-$ cells represented the airways

populations, $CD3^{+}CD4^{+}CD44^{hi}Tetramer^{+}CD45.2\text{-}v500^{-}CD45.2\text{-}BV605^{+}$ represented the vasculature populations and $CD3^{+}CD4^{+}CD44^{hi}Tetramer^{+}CD45.2\text{-}v500^{-}CD45.2\text{-}BV605^{-}$ represented the parenchyma populations. These three populations were further analysed for expression of IL-17, IFN-γ, CXCR3, CD103 and CCR8.

Supplementary figure 3. Mucosal delivery of Z-DCs induces $CD4^{+}$ cell activation through epithelial signaling for vaccine-induced immunity. C57BL/6 mice were vaccinated, infected and received Z-DC as described in method. At the time of harvest, the mice were given both anti-CD45.2-v500 and anti-CD45.2-BV605 antibodies through IT and IV route respectively. Lungs were harvested and subjected to flow cytometry. The number of $CD4^{+}CD44^{hi}$ T cells were detected by flow cytometry (**A**). The distribution of $CD4^{+}CD44^{hi}$ T cells (**B**) in *Mtb*-infected BCG vaccinated mice and *Mtb*-infected BCG vaccinated mice that received Z-DC transfer were measured in lung airways (red bar), parenchyma (blue bar) and vasculature (green bar) regions by flow cytometry. n =4-5 mice per group. Gating strategy is shown to detect myeloid cell populations (**C**). AMs were characterised as $CD11C^{+}CD11B^{-}SiglecF^{+}$, RMs were characterised as $CD11C^{-}CD11B^{+}Gr1^{-}$. AMs and RMs were further characterised based on the expression of CD45.2-v500 and CD45.2-BV605 to determine their location as mentioned above. B6, and *Cd103*$^{-/-}$ mice were vaccinated, infected and received Z-DC as described in method. Mice were harvested at 20 dpi and lung bacterial burden was determined by plating **(D)**. n =4-5 mice per group. In a separate experiment, *Ikk*$^{fl/fl}$*Sftp*^{cre} mice were vaccinated, infected and received Z-DC as described in method. To track the immune cells mice were given anti-CD45.2-v500 and anti-CD45.2-BV605 antibodies as before. Lungs were harvested at 20 dpi and MHC-II MFI (mean fluorescent intensity-MFI) on RMs (**E**), the total numbers of $CD4^{+}CD44^{hi}$ (**F**), $CD4^{+}CD44^{hi}TET^{+}$ T (**G**) cells were determined by flow cytometry (red=*Ikk*$^{fl/fl}$, blue= *Ikk*$^{fl/fl}$*Sftp*^{cre}*)*. n=4-5 mice per group. Data represented as mean ± SD. ** p≤ 0.01, *** p≤0.001, ****p≤ 0.0001 either by two way ANOVA (**A and B**), or Student's t test (actual p values are shown) (**D-G**).

Supplementary Table legends:

Table S1: Description of Cell proportion in each cluster per condition from scRNA-seq analysis.

Table S2: Description of TCRs per condition from scRNA-seq analysis.

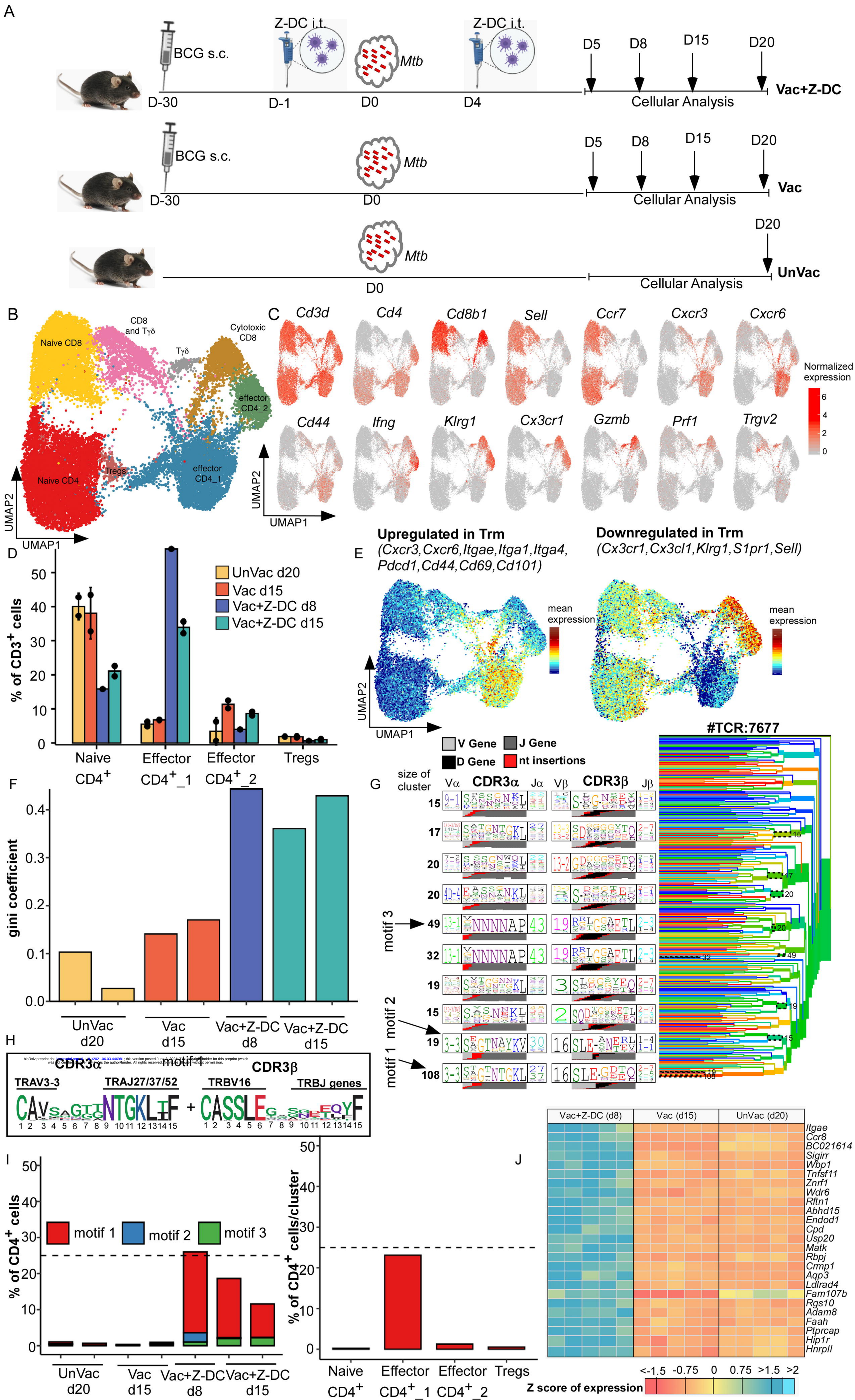
A
BCG s.c.
Z-DC i.t.
Mtb
Z-DC i.t.
D5
D8
D15
D20
D-30
D-1
D0
D4
Cellular Analysis
Vac+Z-DC
BCG s.c.
Mtb
D5
D8
D15
D20
D-30
D0
Cellular Analysis
Vac
Mtb
D20
D0
Cellular Analysis
UnVac
B
CD8 and Tγδ
Cytotoxic CD8
Naive CD8
Tγδ
effector CD4_2
Naive CD4
Tregs
effector CD4_1
UMAP2
UMAP1
C
Cd3d
Cd4
Cd8b1
Sell
Ccr7
Cxcr3
Cxcr6
Cd44
Ifng
Klrg1
Cx3cr1
Gzmb
Prf1
Trgv2
Normalized expression
6
4
2
0
D
% of CD3+ cells
UnVac d20
Vac d15
Vac+Z-DC d8
Vac+Z-DC d15
Naive CD4+
Effector CD4+_1
Effector CD4+_2
Tregs
E
Upregulated in Trm
(Cxcr3,Cxcr6,Itgae,Itga1,Itga4,
Pdcd1,Cd44,Cd69,Cd101)
Downregulated in Trm
(Cx3cr1,Cx3cl1,Klrg1,S1pr1,Sell)
mean expression
mean expression
UMAP2
UMAP1
F
gini coefficient
UnVac d20
Vac d15
Vac+Z-DC d8
Vac+Z-DC d15
G
#TCR:7677
V Gene
J Gene
D Gene
nt insertions
size of cluster
Vα
CDR3α
Jα
Vβ
CDR3β
Jβ
15
17
20
20
49
32
19
15
19
108
motif 3
motif 2
motif 1
H
bioRxiv preprint doi: https://doi.org/10.1101/2021.06.03.446981; this version posted June 3, 2021. The copyright holder for this preprint (which was not certified by peer review) is the author/funder. All rights reserved. No reuse allowed without permission.
CDR3α
motif 1
CDR3β
TRAV3-3
TRAJ27/37/52
TRBV16
TRBJ genes
I
% of CD4+ cells
motif 1
motif 2
motif 3
UnVac d20
Vac d15
Vac+Z-DC d8
Vac+Z-DC d15
J
% of CD4+ cells/cluster
Naive CD4+
Effector CD4+_1
Effector CD4+_2
Tregs
Vac+Z-DC (d8)
Vac (d15)
UnVac (d20)
Itgae
Ccr8
BC021614
Sigirr
Wbp1
Tnfsf11
Znrf1
Wdr6
Rftn1
Abhd15
Endod1
Cpd
Usp20
Matk
Rbpj
Crmp1
Aqp3
Ldlrad4
Fam107b
Rgs10
Adam8
Faah
Ptprcap
Hip1r
Hnrpll
<-1.5
-0.75
0
0.75
>1.5
>2
Z score of expression